Spin Hall Effect and Multi-orbital Kondo Scattering

Guang-Yu Guo (郭光宇)

Physics Department, National Taiwan University

(國立臺灣大學物理系)

Physics Division, National Center for Theoretical Sciences

(國家理論科學中心物理組)

(NCTS Mini-workshop "Frontier Topics on Topology, Non-Fermi Liquid and Strong Correlations in Quantum Many-body Systems", National Chiao-Tung Univ., March 3, 2016)

Plan of this Talk

I. Introduction

1. Spin Hall effect
2. Motivations

II. Intrinsic spin Hall effect in metals

1. Linear response Kubo formalism
2. Berry phase formalism
3. Large intrinsic spin Hall effect in platinum
4. Intrinsic spin Hall effect in pure Pd, Au and Mo metals

III. Gigantic spin Hall effect in gold and multi-orbital Kondo effect

1. Gigantic spin Hall effect in gold
2. Multi-orbital Kondo effect in Fe impurity in gold.
3. Enhanced SHE by resonant skew scattering in orbital-dependent Kondo effect.
4. Quantum Monte Carlo simulation of multi-orbital Kondo effect

IV. Conclusions and On-going Work

I. Introduction

1. Spin Hall effect

1) Ordinal Hall Effect

Lorentz force

$q\mathbf{v}\times\mathbf{B}$

[Hall 1879]

$$\rho_{\mathrm{Hall}} = R_0 B$$

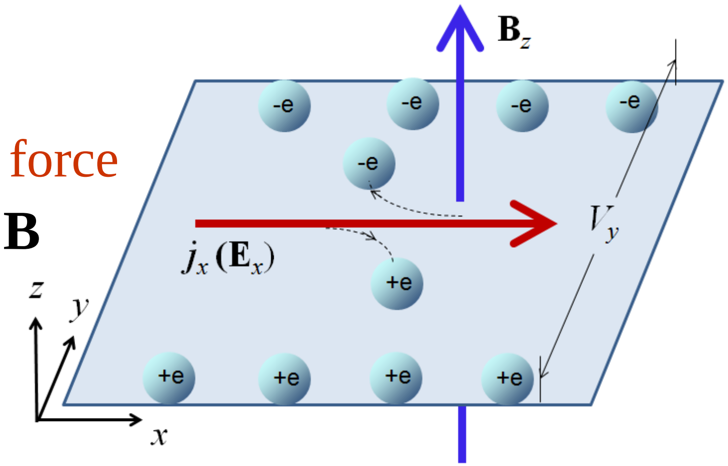

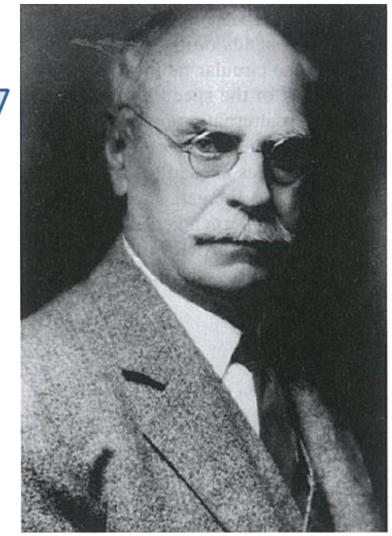

Edwin H. Hall (1855-1938)

2) Anomalous Hall Effect [Hall, 1880 & 1881]

$$\rho_{\mathrm{Hall}} = R_0 B + R_S M$$

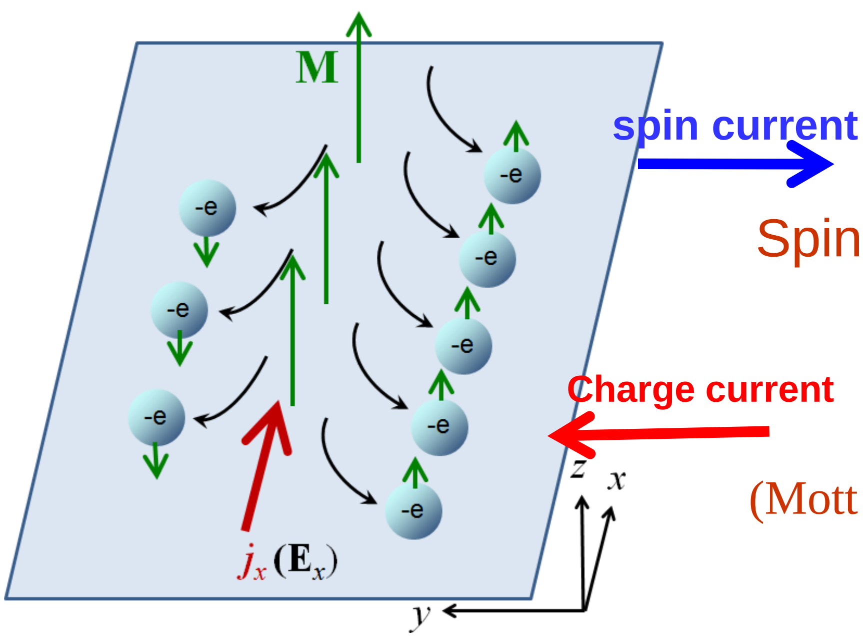

3) (extrinsic) Spin Hall Effect

[Dyakonov & Perel, JETP 1971;
Hirsch, PRL 1999; Zhang, PRL 2000]

Spin-orbit interaction

$$\frac{dV(r)}{dr}(\mathbf{s}\cdot\mathbf{L})$$

(Mott or skew scattering)

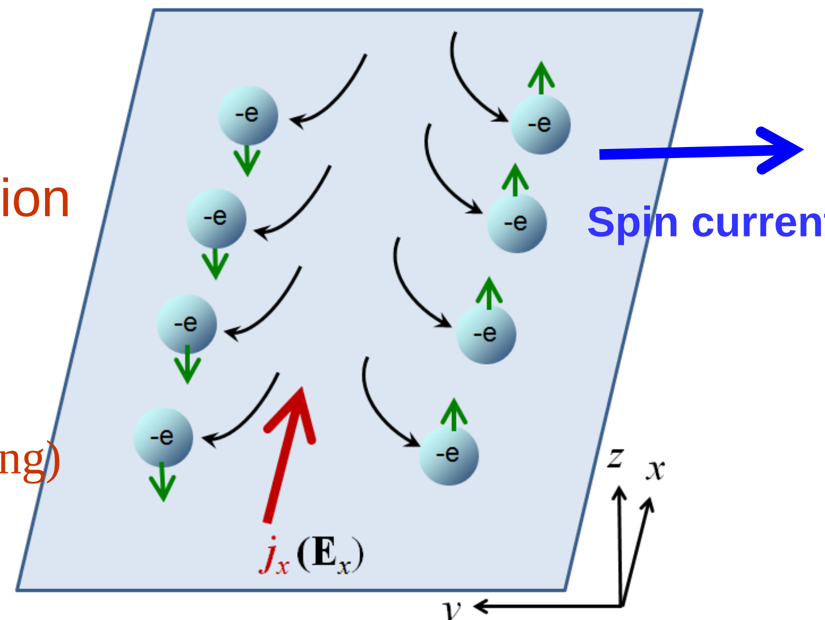

4) Intrinsic spin Hall effect

(1) In p-type zincblende semiconductors

Dissipationless Quantum Spin Current at Room Temperature

Shuichi Murakami,[1*] Naoto Nagaosa,[1,2,3] Shou-Cheng Zhang[4]

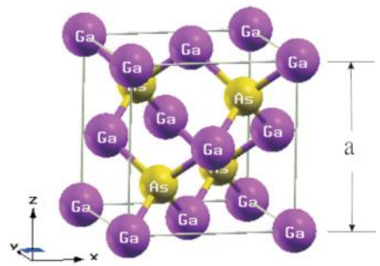

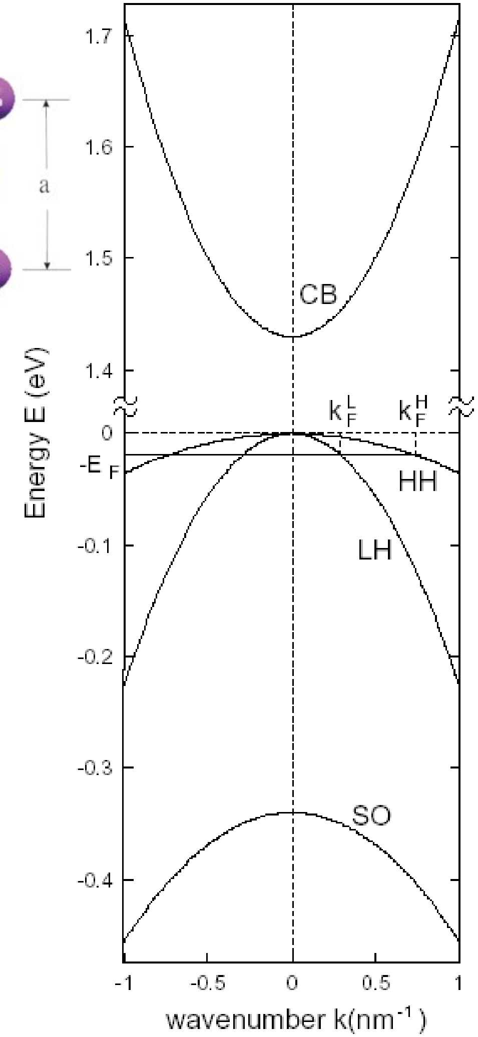

Luttinger model $$H_0 = \frac{\hbar^2}{2m}\left[(\gamma_1 + \frac{5}{2}\gamma_2)k^2 - 2\gamma_2(\vec{k}\cdot\vec{S})^2\right]$$

Equation of motion $$\left\langle \dot{X}_i \right\rangle = \frac{\hbar k_i}{m_\lambda} + F_{il}\left\langle \dot{k}_l \right\rangle$$

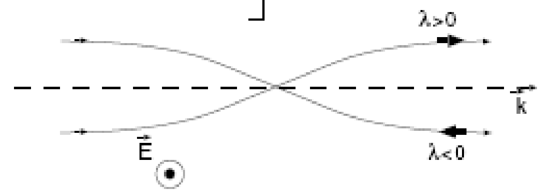

$$\left\langle \dot{k}_i \right\rangle = \frac{e}{\hbar}E_i \qquad e > 0 \text{ (hole)}$$

Anomalous velocity $$\left\langle \dot{\vec{X}} \right\rangle = \frac{\hbar\vec{k}}{m_\lambda} - \frac{e\lambda}{\hbar k^3}\vec{k}\times\vec{E}$$

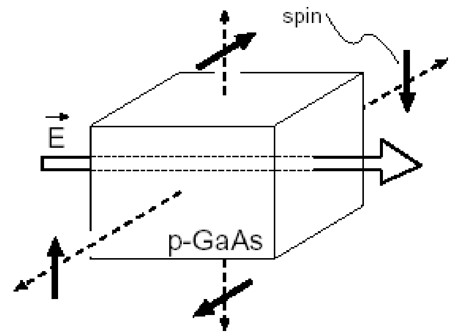

$$j_j^i = \sigma_s \varepsilon^{ijk} E_k \qquad (1)$$

$$j_y^x = \frac{eE_z}{12\pi^2}(3k_F^{\mathrm{H}} - k_F^{\mathrm{L}}) = \frac{\hbar}{2e}\sigma_s E_z \quad (10)$$

$n_h = 10^{19}$ cm^{-3}, μ= 50 cm /V ·s, σ= $e\mu n_h$ = 80 Ω^{-1}cm^{-1};
σ_s= 80 Ω^{-1}cm^{-1}

$n_h = 10^{16}$ cm^{-3}, μ= 50 cm /V ·s, σ= $e\mu n_h$ = 0.6 Ω^{-1}cm^{-1};
σ_s= 7 Ω^{-1}cm^{-1}

(2) In a 2-D electron gas in n-type semiconductor heterostructures

Universal Intrinsic Spin Hall Effect

[PRL 92, 126603]

Jairo Sinova,[1,2] Dimitrie Culcer,[2] Q. Niu,[2] N. A. Sinitsyn,[1] T. Jungwirth,[2,3] and A. H. MacDonald[2]

Rashba Hamiltonian

$$H = \frac{p^2}{2m} - \frac{\lambda}{\hbar}\vec{\sigma}\cdot(\hat{z}\times\vec{p}), \qquad (1)$$

contributes to the spin current. In this case we find that the spin current in the $\hat{y}$ direction is [23]

$$j_{s,y} = \int_{\text{annulus}} \frac{d^2\vec{p}}{(2\pi\hbar)^2}\frac{\hbar n_{z,\vec{p}}}{2}\frac{p_y}{m} = \frac{-eE_x}{16\pi\lambda m}(p_{F+} - p_{F-}), \qquad (6)$$

where p_{F+} and p_{F-} are the Fermi momenta of the majority and minority spin Rashba bands. We find that when both bands are occupied, i.e., when $n_{2D} > m^2\lambda^2/\pi\hbar^4 \equiv n^*_{2D}$, $p_{F+} - p_{F-} = 2m\lambda/\hbar$ and then the spin Hall (sH) conductivity is

Universal spin Hall conductivity

$$\sigma_{sH} \equiv -\frac{j_{s,y}}{E_x} = \frac{e}{8\pi}, \qquad (7)$$

independent of both the Rashba coupling strength and of the 2DES density. For $n_{2D} < n^*_{2D}$ the upper Rashba band is depopulated. In this limit p_{F-} and p_{F+} are the interior and exterior Fermi radii of the lowest Rashba split band, and σ_{sH} vanishes linearly with the 2DES density:

$$\sigma_{sH} = \frac{e}{8\pi}\frac{n_{2D}}{n^*_{2D}}. \qquad (8)$$

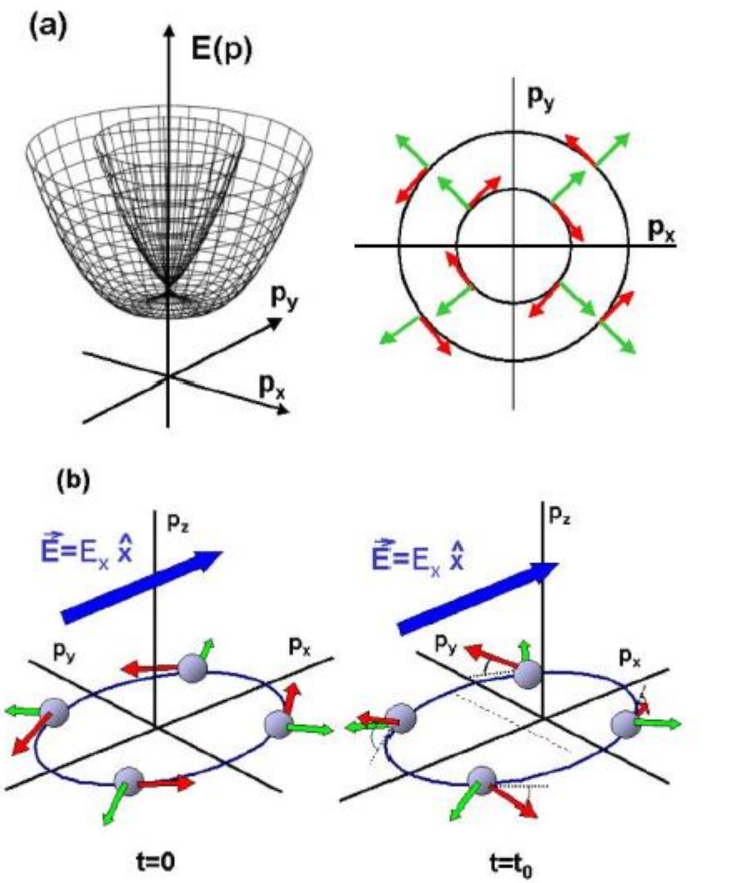

(3) Significances of these theoretical discoveries of intrinsic spin Hall effects

Basic elements of spintronics (spin electronics):

Generation, detection, & manipulation of spin current.

Usual spin current generations:

Ferromagnetic leads

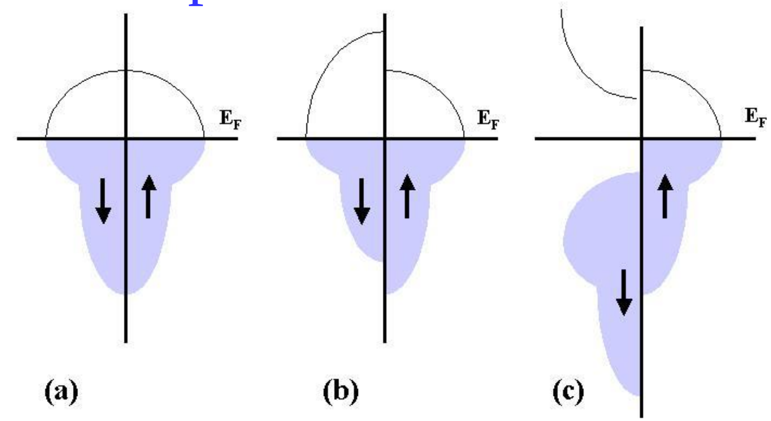

(a) non-magnetic metals, (b) ferromagnetic metals and (c) half-metallic metals.

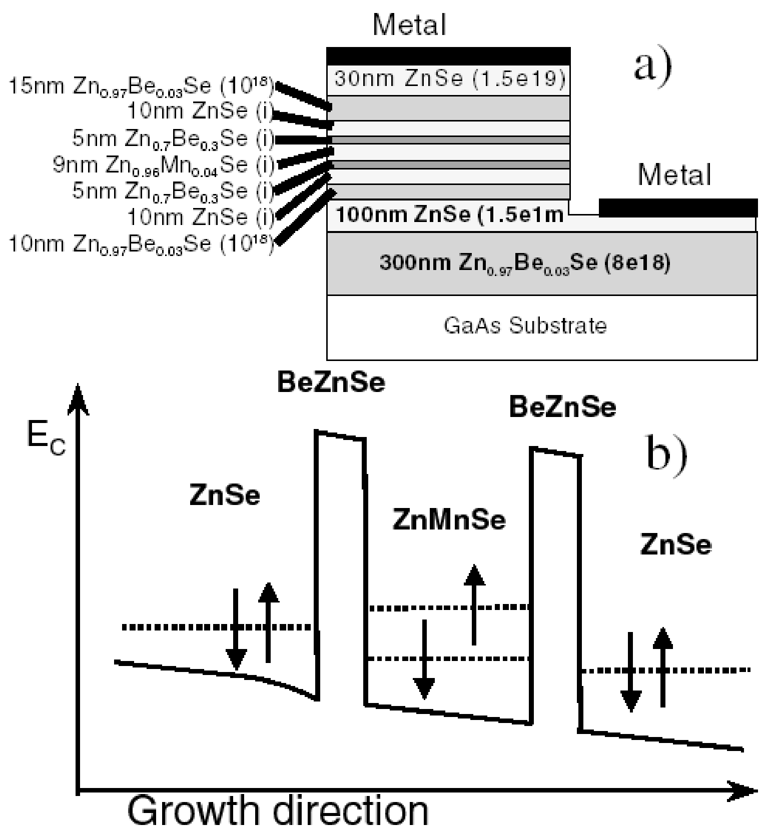

FIG. 1. (a) Layer structure of the device and (b) schematic view of resonant tunnel diode band structure under bias.

Spin filter

[Slobodskyy, et al., PRL 2003]

Problems: magnets and/or magnetic fields needed, and difficult to integrate with semiconductor technologies.

It would allow to generate spin current electrically in semiconductor microstructures without applied magnetic fields or magnetic materials, and make possible pure electric driven spintronics which could be readily integated with conventional electronics.

5) Experiments on spin Hall effect

(a) in n-type 3D GaAs and InGaAs thin films

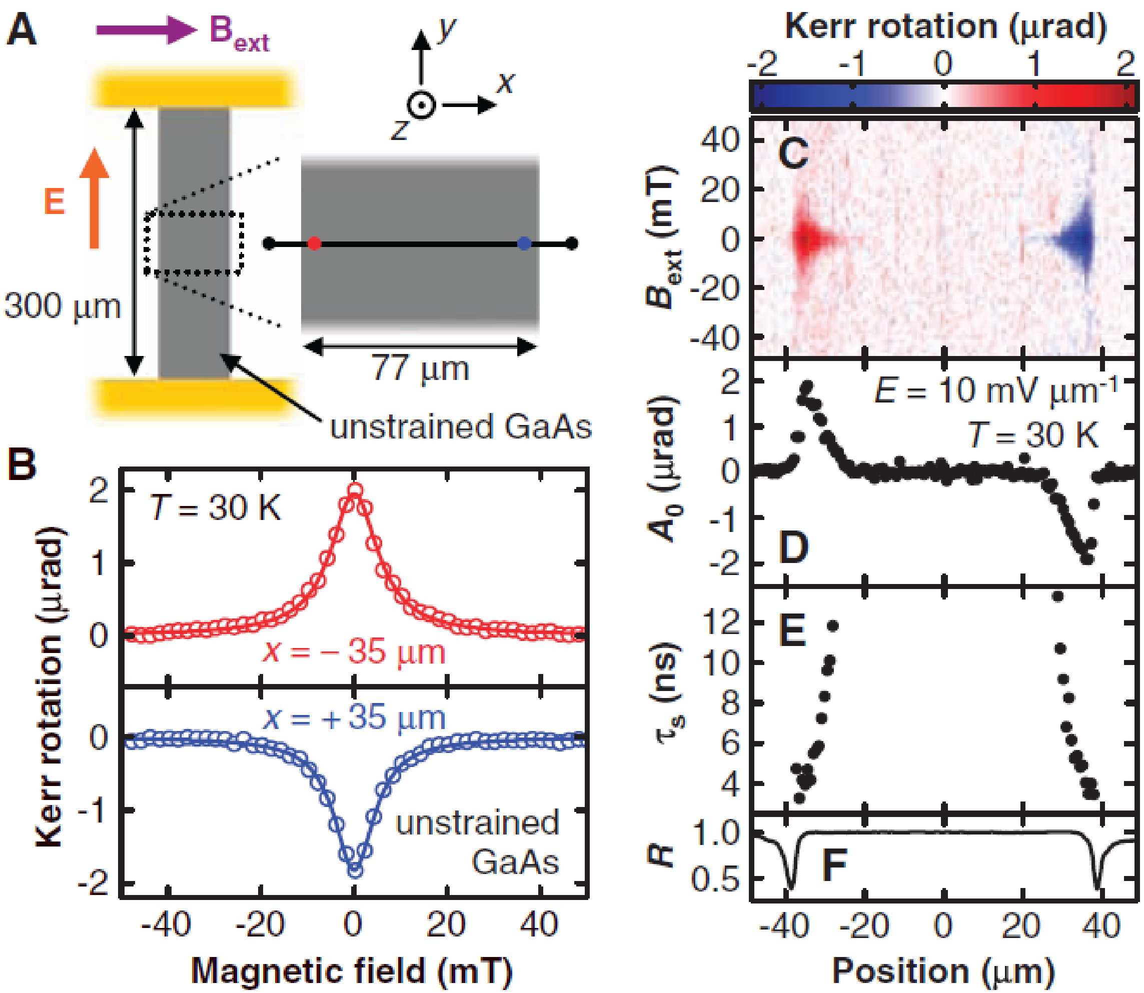

[Kato *et al.*, Science 306, 1910 (2004)]

Attributed to extrinsic SHE because of weak crystal direction dependence.

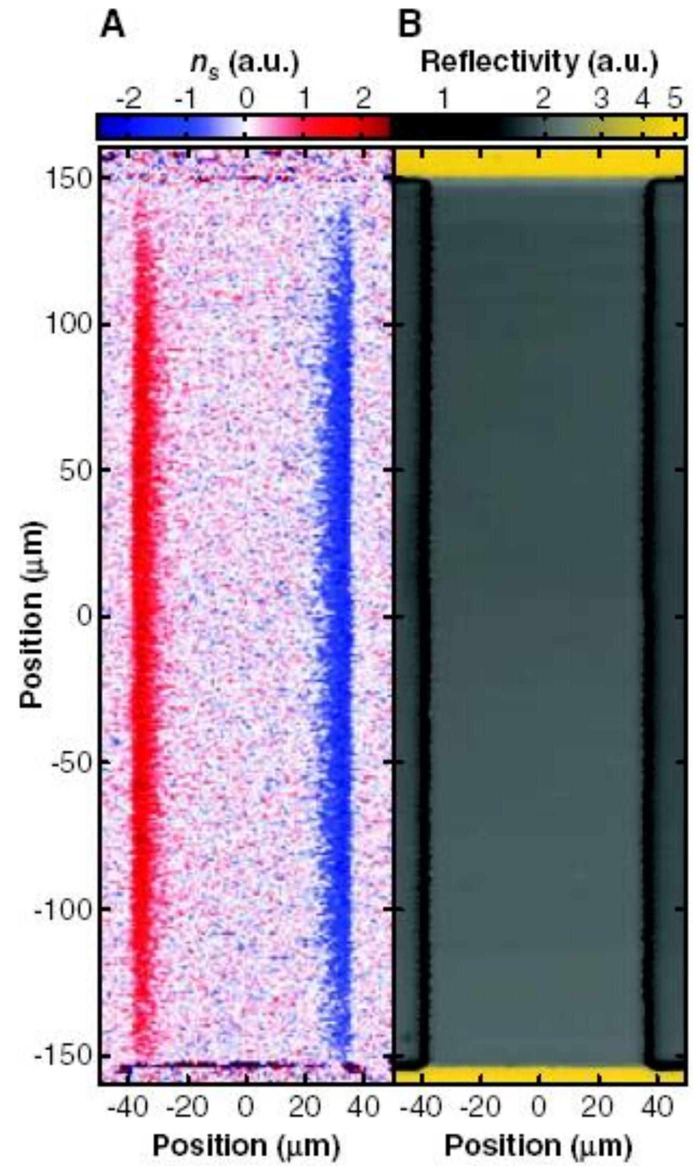

Fig. 2. (**A** and **B**) Two-dimensional images of spin density n_s and reflectivity R, respectively, for the unstrained GaAs sample measured at T = 30 K and E = 10 mV μm^{-1}.

(b) in p-type 2D semiconductor quantum wells

Experimental Observation of the Spin-Hall Effect in a Two-Dimensional Spin-Orbit Coupled Semiconductor System [PRL 94 (2005) 047204]

J. Wunderlich,[1] B. Kaestner,[1,2] J. Sinova,[3] and T. Jungwirth[4,5]

We report the experimental observation of the spin-Hall effect in a 2D hole system with spin-orbit coupling. The 2D hole layer is a part of a *p-n* junction light-emitting diode with a specially designed coplanar geometry which allows an angle-resolved polarization detection at opposite edges of the 2D hole system. In equilibrium the angular momenta of the spin-orbit split heavy-hole states lie in the plane of the 2D layer. When an electric field is applied across the hole channel, a nonzero out-of-plane component of the angular momentum is detected whose sign depends on the sign of the electric field and is opposite for the two edges. Microscopic quantum transport calculations show only a weak effect of disorder, suggesting that the clean limit spin-Hall conductance description (intrinsic spin-Hall effect) might apply to our system.

Attributed to intrinsic SHE.

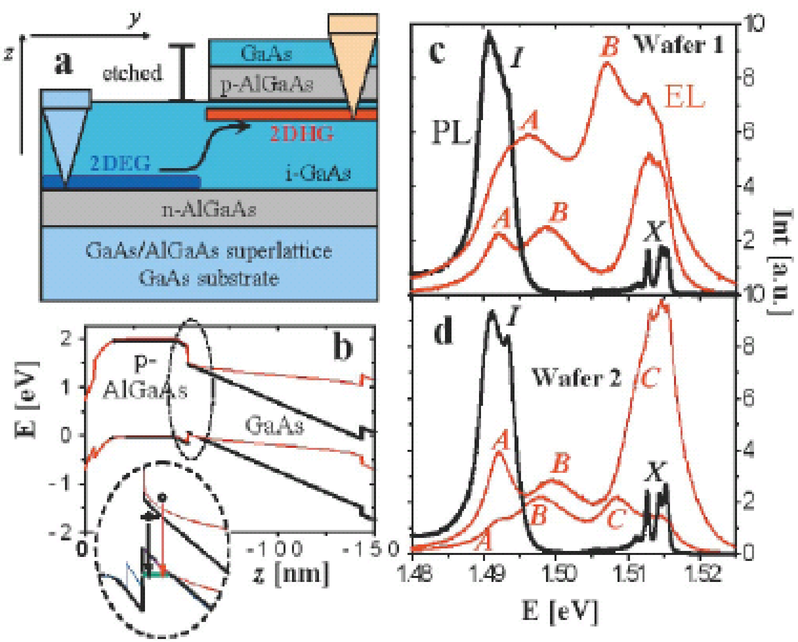

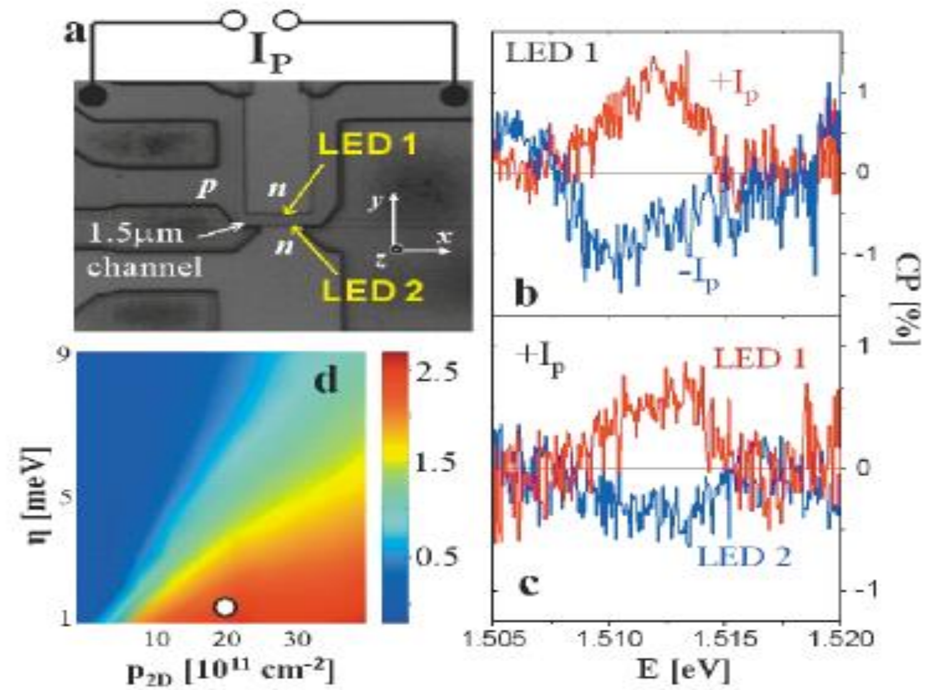

(c) Spin Hall effect in strained *n*-type wurtzite semiconductors

[Chang, Chen, Chen, Hong, Tsai, Chen, Guo, PRL 98, 136403 (2007)]

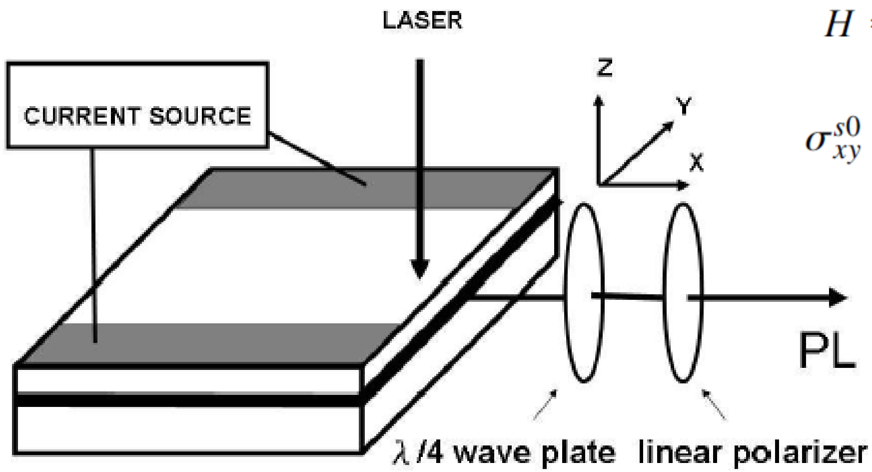

$$H = \frac{\hbar k^2}{2m} + (\alpha_e + \beta k^2)(\sigma_x k_y - \sigma_y k_x)$$

$$\sigma_{xy}^{s0} = -\sigma_{yx}^{s0} \approx \frac{e}{8\pi}\left[1 + \frac{2}{3}\alpha_e\beta\left(\frac{2m}{\hbar^2}\right)^2\right]$$

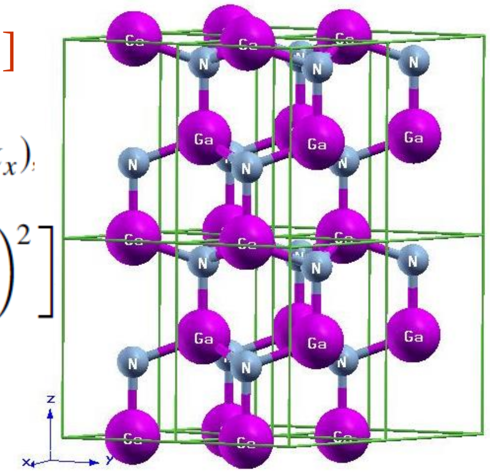

n-type (5nm $In_xGa_{1-x}N$/3nm GaN) superlattice (x=0.15)

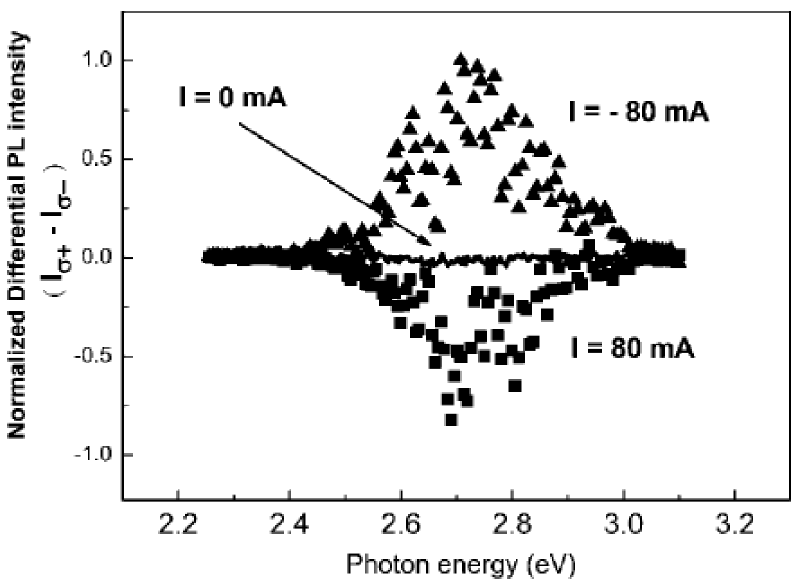

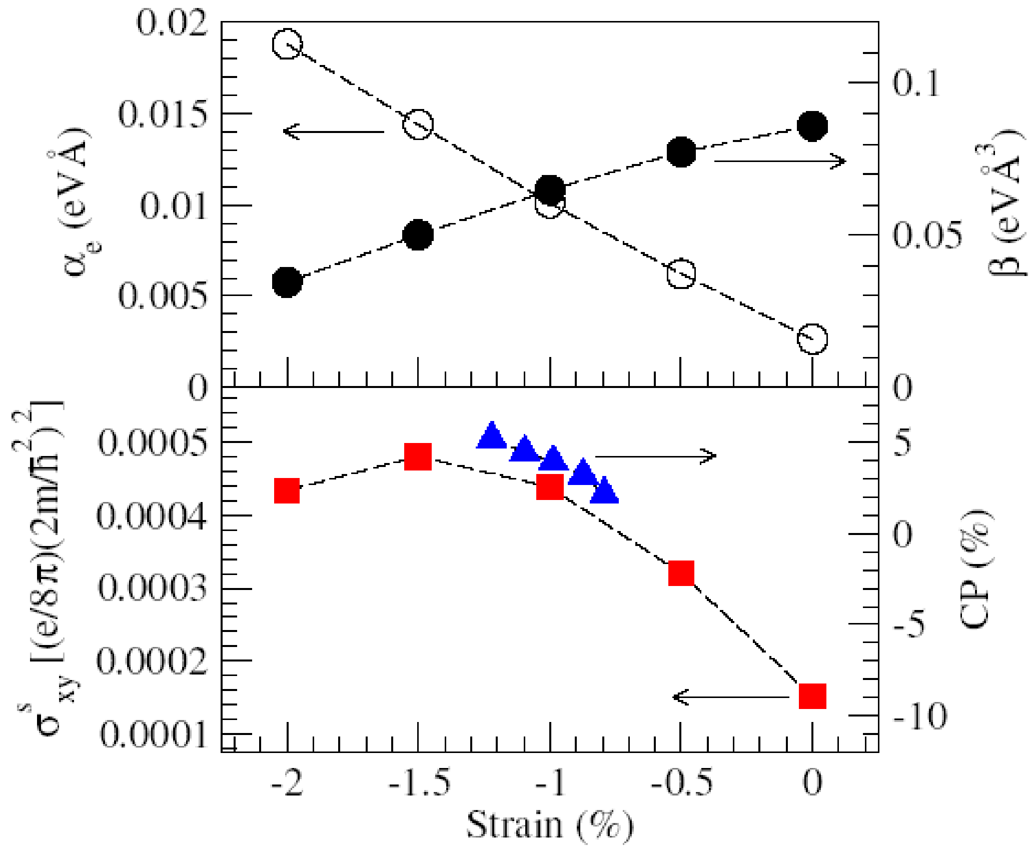

2. Motivations

1) Spin Hall effect in metals

Direct electronic measurement of the spin Hall effect fcc Al Nature 13 July 2006 Vol. 442, P. 04937

(direct) spin Hall effect

S. O. Valenzuela[1]† & M. Tinkham[1]

$$R_{\mathrm{SH}} = \frac{\Delta R_{\mathrm{SH}}}{2}\sin\theta$$

$$\Delta R_{\mathrm{SH}} = \frac{P}{t_{\mathrm{Al}}}\frac{\sigma_{\mathrm{SH}}}{\sigma_c^2}\exp(-L_{\mathrm{SH}}/\lambda_{\mathrm{sf}})$$

σ_{sH} = 27~34 $(\Omega\mathrm{cm})^{-1}$
(T= 4.2 K)

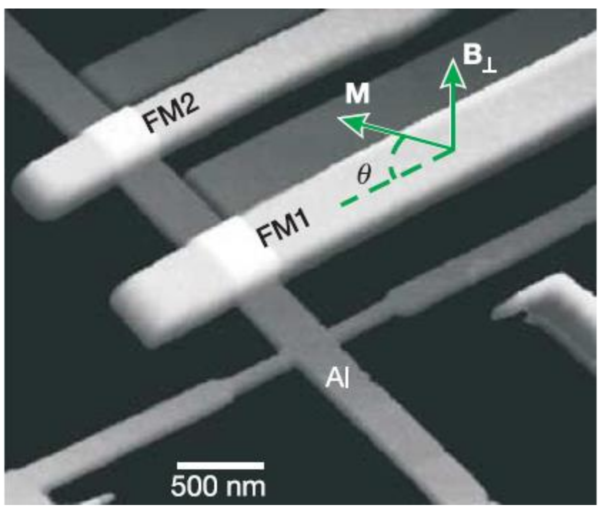

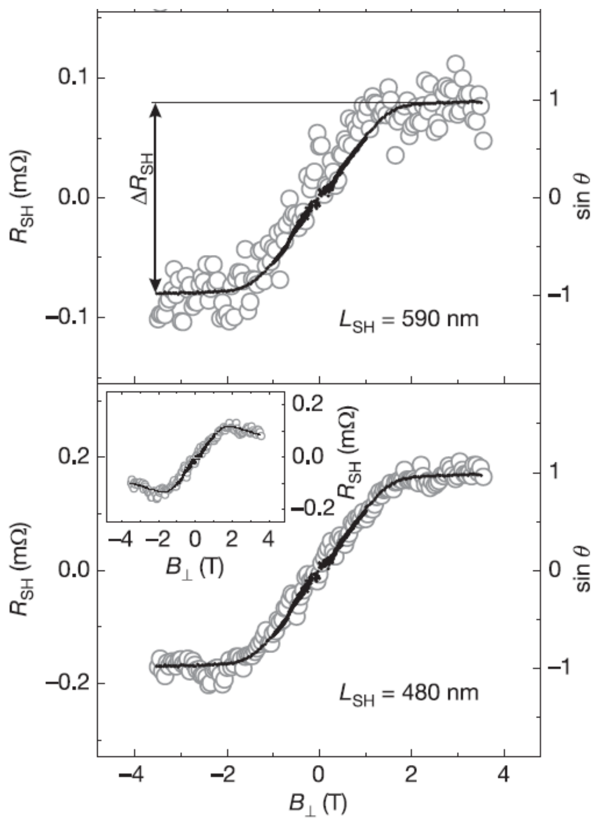

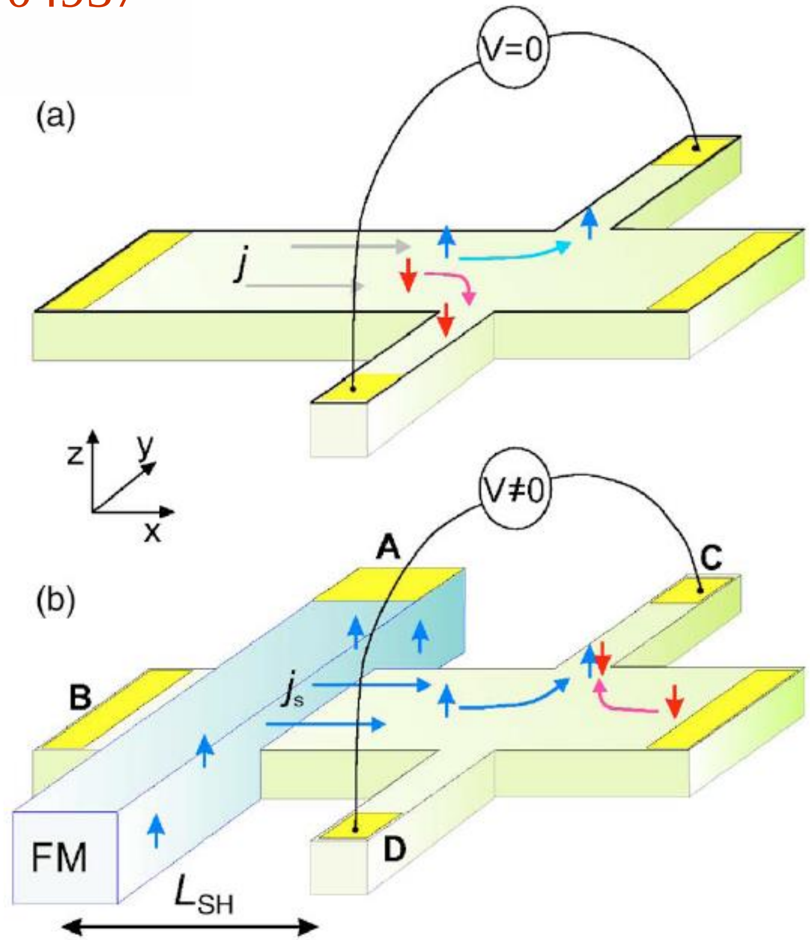

inverse spin Hall effect

Conversion of spin current into charge current at room temperature: Inverse spin-Hall effect

[Saitoh, et al.,
APL 88 (2006) 182509]

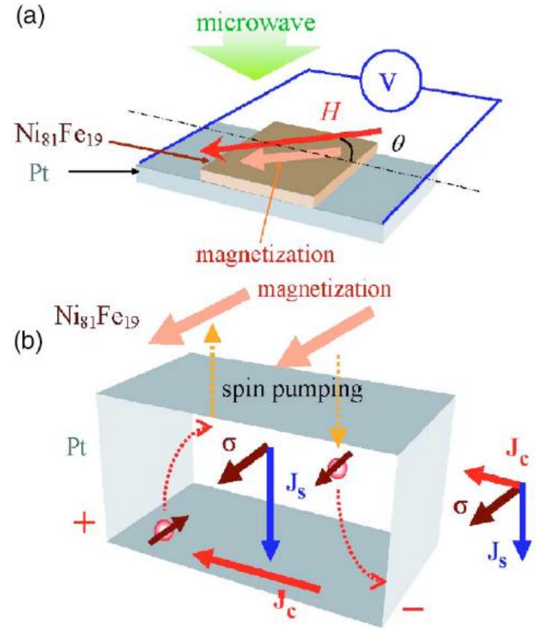

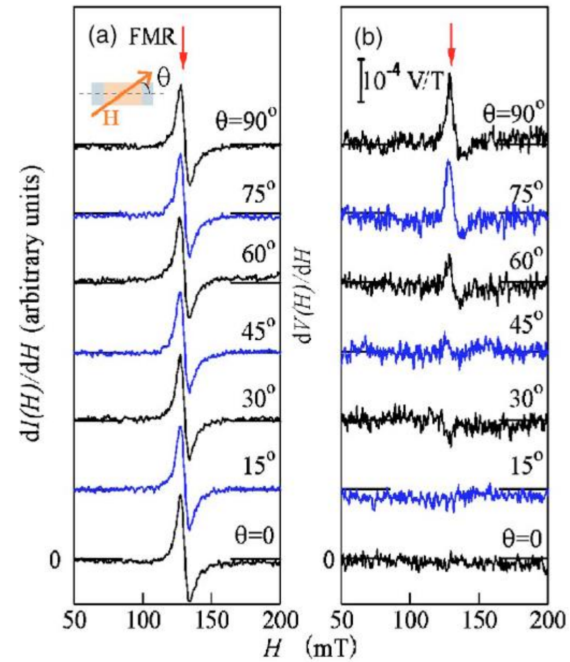

Room-Temperature Reversible Spin Hall Effect

[PRL98, 156601; 98, 139901 (E) (2007)]

T. Kimura,[1,2] Y. Otani,[1,2] T. Sato,[1] S. Takahashi,[3,4] and S. Maekawa[3]

$\sigma_{sH} = 240\ (\Omega\mathrm{cm})^{-1}$
(T= 290 K)

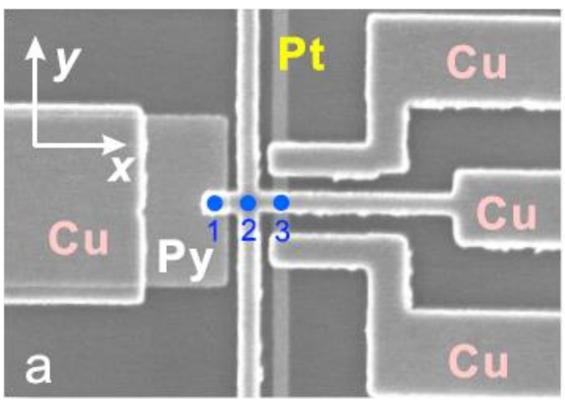

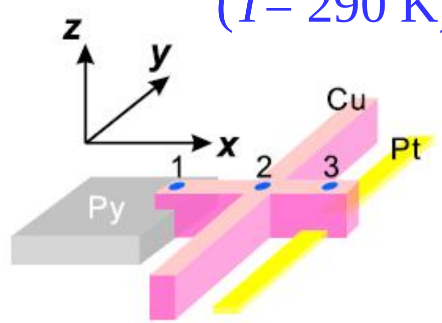

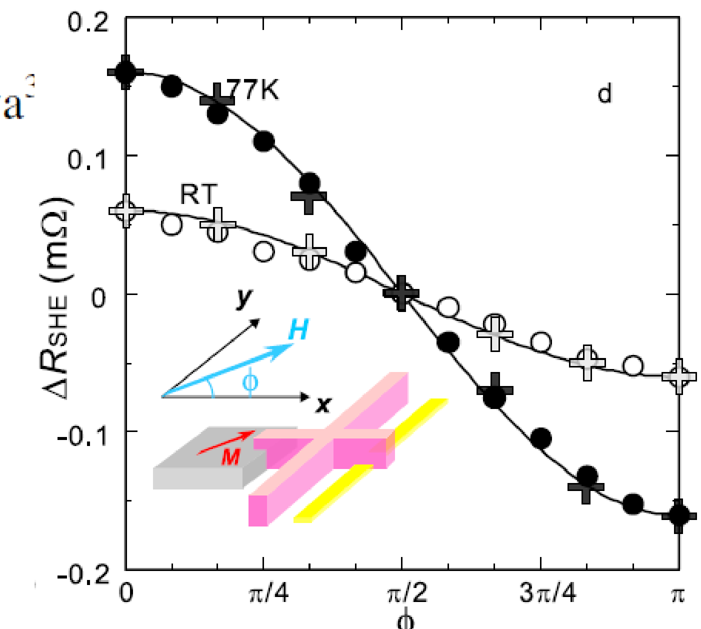

Assumed to be extrinsic!

2) Applications of Spin Hall effect

Spin-Torgue Switching with the Giant Spin Hall Effect of Tantalum

[L. Liu et al., Science 336, 555 (2012)]

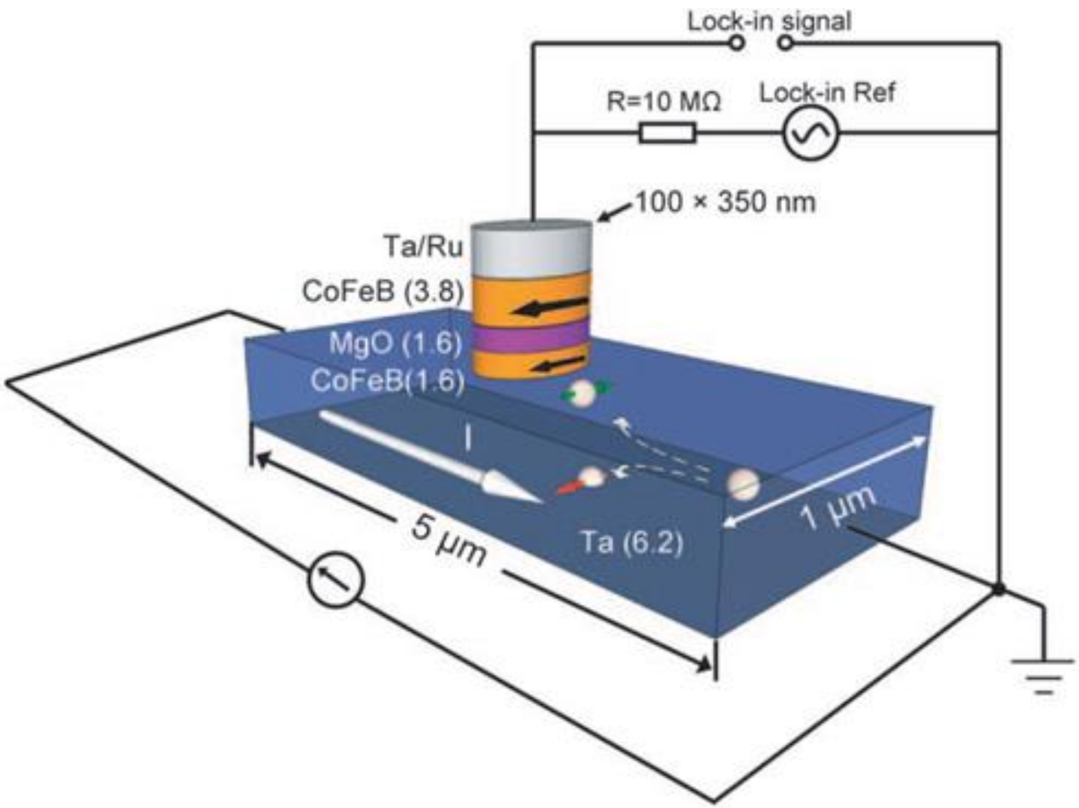

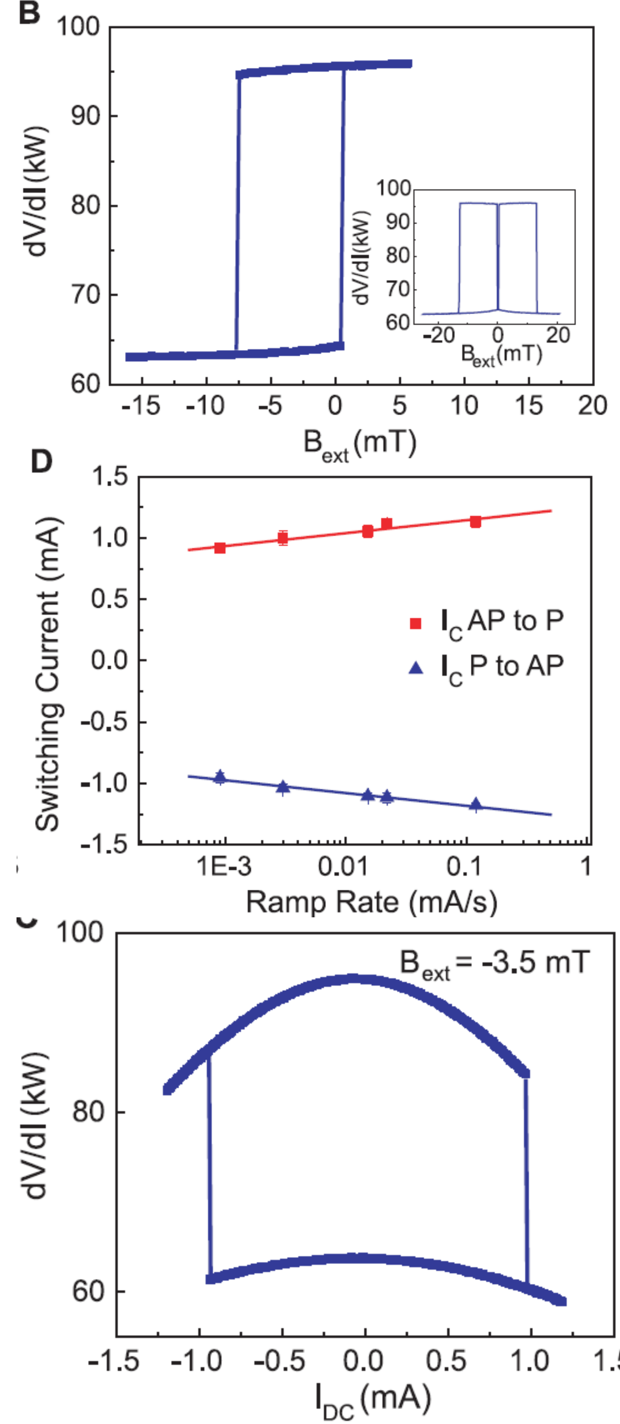

3) Motivations

Advantages of spin Hall effect in metals:

(1) A contact with a ferromagnetic metal does not suffer from conductance mismatch.
(2) Spin Hall conductance is large.
(3) The Fermi temperature is much higher than room temperature and hence quantum coherence is robust again thermal agitations.

Thus, it is important to understand the detailed mechanism of the SHE in metals because it would lead to the material design of the large SHE even at room temperature with the application to the spintronic devices.

II. Intrinsic spin Hall effect in metals

1. Linear response Kubo formalism

[Guo,et al., PRL 94, 226601 (2005)]

Assume E-field along *y*-axis and spin or H-field along *z*-axis, the optical Hall conductivity (off-diagonal element) is [e.g., Marder, 2000]

$$\sigma_{xy}(\omega) = \frac{e}{i\omega V_c}\sum_{\mathbf{k}}\sum_{n\neq n'}(f_{\mathbf{k}n} - f_{\mathbf{k}n'})\frac{\langle \mathbf{k}n|\, j_x\,|\mathbf{k}n'\rangle\langle \mathbf{k}n'|\, v_y\,|\mathbf{k}n\rangle}{\varepsilon_{\mathbf{k}n} - \varepsilon_{\mathbf{k}n'} + \hbar\omega + i\eta}$$

where V_c is the cell volume, $|\mathbf{k}n>$ is the *n*th Bloch state with crystal momentum **k**, $\hbar\omega$ is the photon energy.

Setting η to zero and using

$$\lim_{\eta\to 0}\frac{1}{\omega \pm i\eta} = \mathrm{P}\frac{1}{\omega} \mp i\pi\delta(\omega)$$

Imaginary (part) Hall conductivity

$$\sigma''_{xy}(\omega) = \frac{\pi e}{\omega V_c}\sum_{\mathbf{k}}\sum_{n\neq n'}(f_{\mathbf{k}n} - f_{\mathbf{k}n'})\,\mathrm{Im}[\langle \mathbf{k}n|\, j_x\,|\mathbf{k}n'\rangle\langle \mathbf{k}n'|\, v_y\,|\mathbf{k}n\rangle]\delta(\varepsilon_{\mathbf{k}n'} - \varepsilon_{\mathbf{k}n} - \hbar\omega)$$

Real (part) Hall conductivity is (Kramers-Kronig transformation)

$$\sigma'_{xy}(\omega) = \frac{2}{\pi}\mathrm{P}\int_0^\infty d\omega'\frac{\omega'\sigma''_{xy}(\omega')}{\omega'^2 - \omega^2}$$

Exactly the same as calculation of magneto-optical properties (e.g., Kerr effect) [e.g., Guo and Ebert, PRB 1995].

Ab initio relativistic band structure methods

Calculations must be based on a relativistic band theory because all the intrinsic Hall effects are caused by spin-orbit coupling.

(1) Relativistic linear muffin-tin orbital (LMTO) method.

[Ebert, PRB 1988; Guo & Ebert, PRB 51, 12633 (1995)]

Dirac Hamiltonian $H_D = c\boldsymbol{\alpha}\cdot\mathbf{p} + mc^2(\beta - I) + v(\mathbf{r})I$

$$\sigma''_{xy}(\omega) = \frac{\pi e}{\omega V_c}\sum_{\mathbf{k}}\sum_{n\neq n'}(f_{\mathbf{k}n} - f_{\mathbf{k}n'})\,\mathrm{Im}[\langle \mathbf{k}n|\, j_x\,|\mathbf{k}n'\rangle\langle \mathbf{k}n'|\, v_y\,|\mathbf{k}n\rangle]\delta(\varepsilon_{\mathbf{k}n'} - \varepsilon_{\mathbf{k}n} - \hbar\omega)$$

current operator $j_x = -ec\alpha_x$ (AHE), (charge current operator)

$j_x = \frac{\hbar}{4}\{\beta\Sigma_z, c\alpha_x\}$ (SHE), (spin current operator)

$j_x = \frac{\hbar}{4}\{\beta L_z, c\alpha_x\}$ (OHE). (orbital current operator)

α, β, Σ are 4×4 Dirac matrices.

Application to intrinsic spin Hall effect in semiconductors

[Guo,Yao,Niu, PRL 94, 226601 (2005)]

Spin and orbital angular momentum Hall effects in p-type zincblende semicoductors

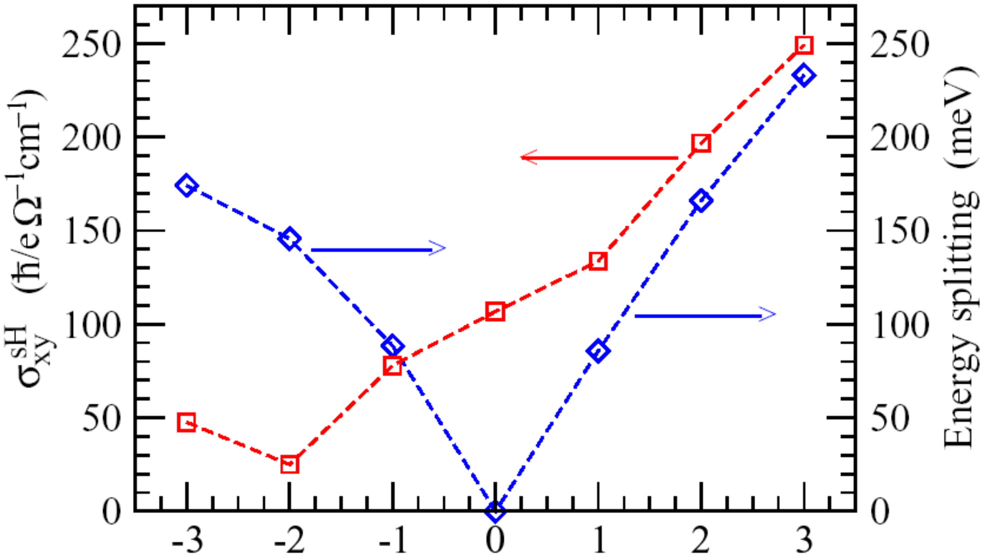

Strain effect

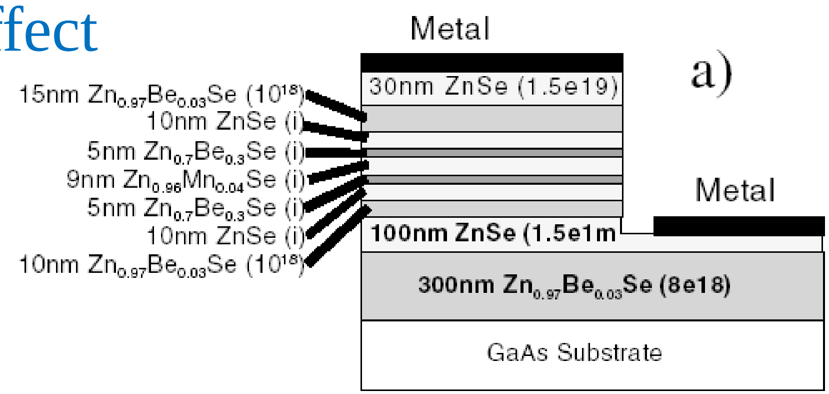

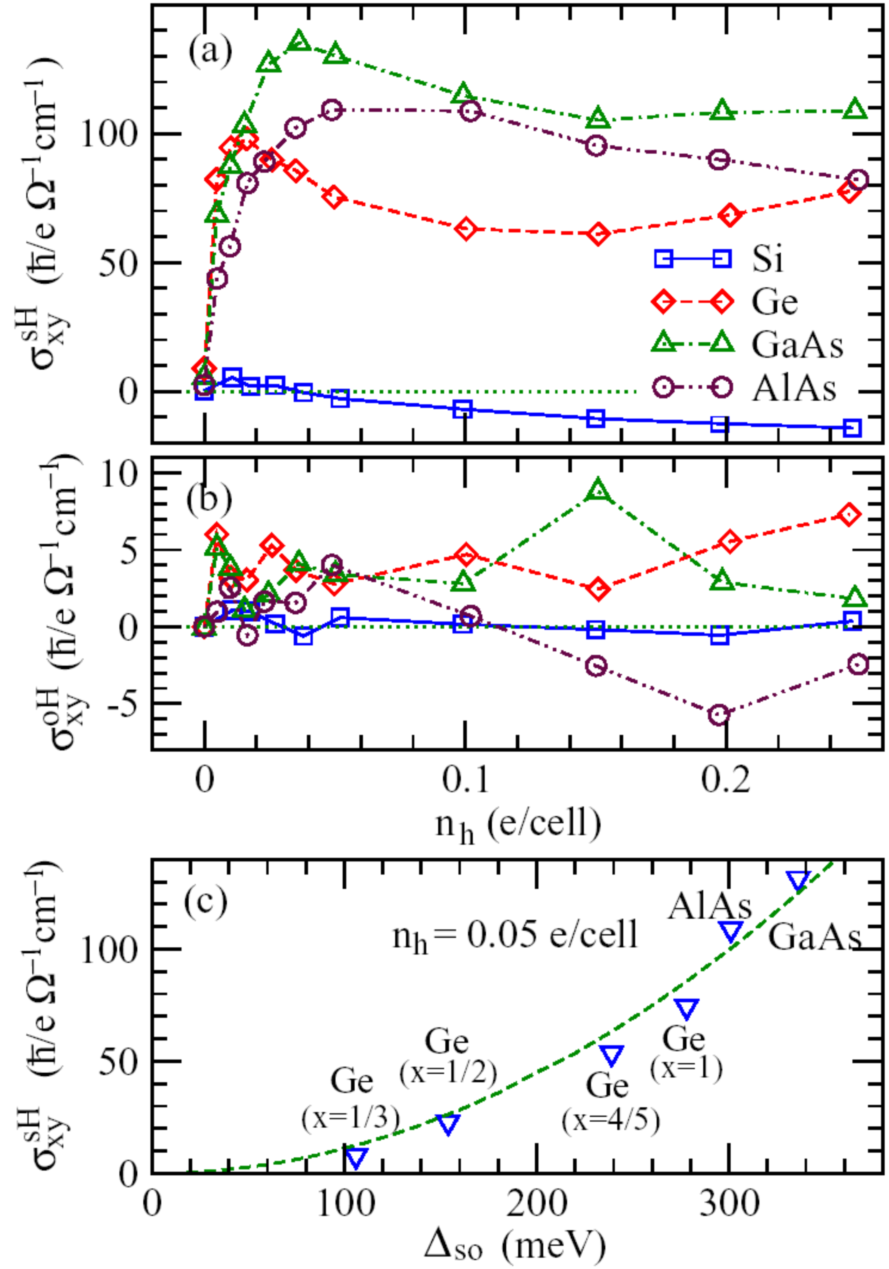

(2) Full-potential linearized augmented plane wave (FLAPW) method as implemented in WIEN2k.

Spin-orbit coupling treated as a perturbation

$$H_P = I\left(-\frac{\hbar^2}{2m}\nabla^2 + v(\mathbf{r})\right) + \sigma_z B(\mathbf{r})$$

$$-I\frac{\hbar^4}{8m^3c^2}\nabla^4 + I\frac{e\hbar^2}{8m^2c^2}\nabla^2 v(\mathbf{r})$$ (scalar relativistic corrections)

$$-\frac{e\hbar}{4m^2c^2}\sigma\bullet(\nabla v(\mathbf{r})\times\mathbf{p})$$ (spin-orbit coupling)

$$\sigma''_{xy}(\omega) = \frac{\pi e}{\omega V_c}\sum_{\mathbf{k}}\sum_{n\neq n'}(f_{\mathbf{k}n} - f_{\mathbf{k}n'})\,\mathrm{Im}[\langle\mathbf{k}n|\,j_x\,|\mathbf{k}n'\rangle\langle\mathbf{k}n'|\,v_y\,|\mathbf{k}n\rangle]\delta(\varepsilon_{\mathbf{k}n'} - \varepsilon_{\mathbf{k}n} - \hbar\omega)$$

current operator $j_x = -ev_x$ (AHE),

$j_x = \hbar\{\sigma_z, v_x\}/4$ (SHE),

$j_x = \hbar\{L_z, v_x\}/4$ (OHE).

2. Berry phase formalism

(1) Semiclassical dynamics of Bloch electrons

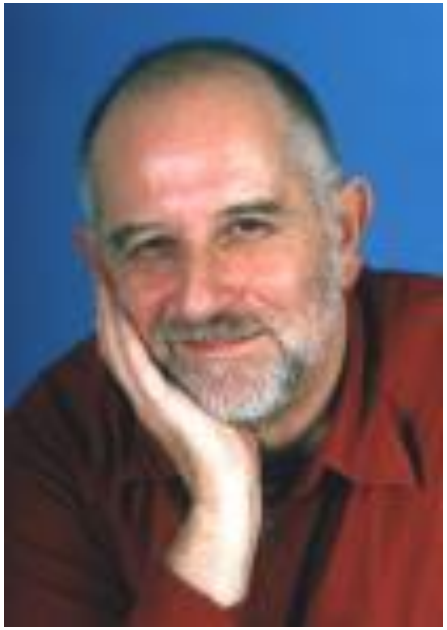

Old version [e.g., Aschroft, Mermin, 1976]

$$\dot{\mathbf{x}}_c = \frac{1}{\hbar}\frac{\partial \varepsilon_n(\mathbf{k})}{\partial \mathbf{k}},$$

$$\dot{\mathbf{k}} = -\frac{e}{\hbar}\mathbf{E} - \frac{e}{\hbar}\dot{\mathbf{x}}_c \times \mathbf{B} = \frac{e}{\hbar}\frac{\partial \varphi(\mathbf{r})}{\partial \mathbf{r}} - \frac{e}{\hbar}\dot{\mathbf{x}}_c \times \mathbf{B}.$$

Berry phase correction [Xiao, Chang & Niu, RMP 82, 1959 (2010)]

New version [Marder, 2000]

$$\dot{\mathbf{x}}_c = \frac{1}{\hbar}\frac{\partial \varepsilon_n(\mathbf{k})}{\partial \mathbf{k}} - \dot{\mathbf{k}} \times \mathbf{\Omega}_n(\mathbf{k}),$$

$$\dot{\mathbf{k}} = \frac{e}{\hbar}\frac{\partial \varphi(\mathbf{r})}{\partial \mathbf{r}} - \frac{e}{\hbar}\dot{\mathbf{x}}_c \times \mathbf{B},$$

$$\mathbf{\Omega}_n(\mathbf{k}) = -\,\mathrm{Im}\left\langle \frac{\partial u_{n\mathbf{k}}}{\partial \mathbf{k}} \middle| \times \middle| \frac{\partial u_{n\mathbf{k}}}{\partial \mathbf{k}} \right\rangle.$$ (Berry curvature)

(2) Semiclassical transport theory

$$\mathbf{j} = \int d^3k(-e\dot{\mathbf{x}})g(\mathbf{r},\mathbf{k}), \qquad g(\mathbf{r},\mathbf{k}) = f(\mathbf{k}) + \delta f(\mathbf{r},\mathbf{k})$$

$$\dot{\mathbf{x}} = \frac{\partial \varepsilon_n(\mathbf{k})}{\hbar \partial \mathbf{k}} + \frac{e}{\hbar}\mathbf{E}\times\mathbf{\Omega}$$

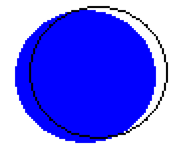

$$\mathbf{j} = -\frac{e^2}{\hbar}\mathbf{E}\times\int d^3\mathbf{k} f(\mathbf{k})\mathbf{\Omega} - \frac{e}{\hbar}\int d^3\mathbf{k}\,\delta f(\mathbf{k},\mathbf{r})\frac{\partial \varepsilon_n(\mathbf{k})}{\partial \mathbf{k}}$$

(Anomalous Hall conductance) (ordinary conductance)

Anomalous Hall conductivity

[Yao, et al., PRL 92 (2004) 037204]

$$\sigma_{xy} = -\frac{e^2}{\hbar}\int d^3\mathbf{k}\sum_n f(\varepsilon_n(\mathbf{k}))\Omega_n^z(\mathbf{k})$$

$$\Omega_n^z(\mathbf{k}) = -\sum_{n'\neq n}\frac{2\,\mathrm{Im}\langle \mathbf{k}n|v_x|\mathbf{k}n'\rangle\langle \mathbf{k}n'|v_y|\mathbf{k}n\rangle}{(\omega_{\mathbf{k}n'}-\omega_{\mathbf{k}n})^2}$$

Intrinsic Hall conductivities

[Yao, et al., PRL 92 (2004) 037204]

[Guo, Murakami, Chen, Nagaosa, PRL100, 096401 (2008)]

$$\sigma_{xy} = \frac{e}{\hbar}\int d^3\mathbf{k}\sum_n f(\varepsilon_n(\mathbf{k}))\Omega_n^z(\mathbf{k})$$

$$\Omega_n^z(\mathbf{k}) = -\sum_{n'\neq n}\frac{2\,\mathrm{Im}\langle \mathbf{k}n|\, j_x\,|\mathbf{k}n'\rangle\langle \mathbf{k}n'|\,v_y\,|\mathbf{k}n\rangle}{(\omega_{\mathbf{k}n}-\omega_{\mathbf{k}n'})^2}$$

current operator

$j_x = -ev_x$ (AHE),

$j_x = \hbar\{\sigma_z, v_x\}/4$ (SHE),

$j_x = \hbar\{L_z, v_x\}/4$ (OHE).

[FLAPW (WIEN2k) calculations]

σ_{xy} (S/cm)	theory	Exp.
bcc Fe	750[a]	1030
hcp Co	477[b]	480
fcc Ni	-1066[c]	-1100

[a] [Yao, et al., PRL 92 (2004) 037204]

[b] [Wang, et al., PRB 76 (2007) 195109]

[c] [Fuh, Guo, PRB 84 (2011) 144427]

3. Large intrinsic spin Hall effect in platinum

Al: σ_{sH} (4.2 K) = 17 $(\Omega\mathrm{cm})^{-1}$

σ_{sH} (exp., 4.2K) = 27, 34 $(\Omega\mathrm{cm})^{-1}$

[Valenzuela, Tinkham, Nature 442, 176 (2006)]

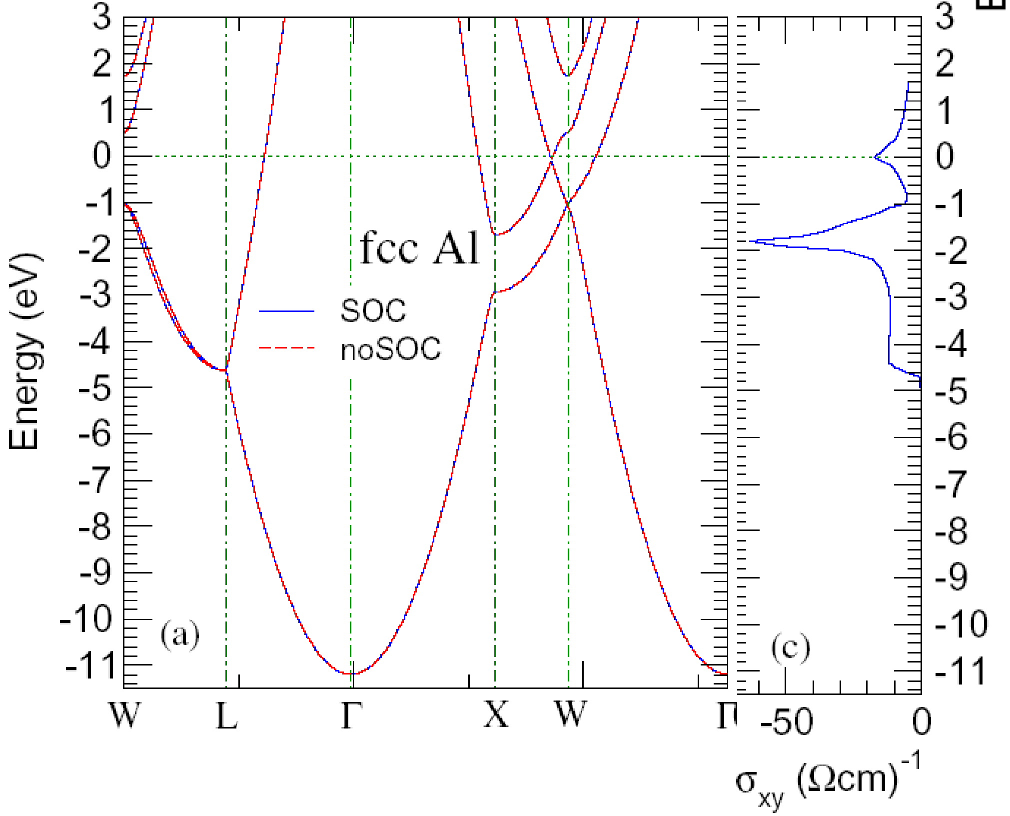

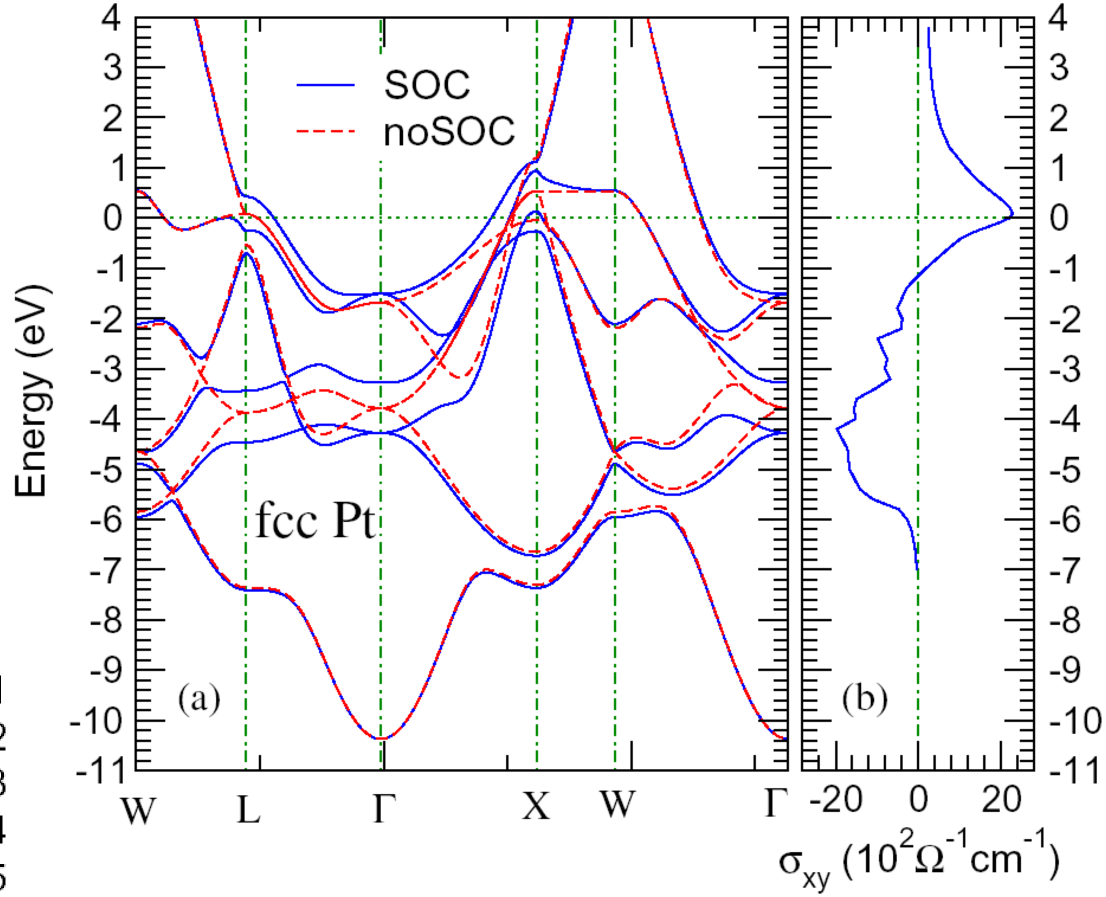

Pt: σ_{sH} = 2200 $(\Omega\mathrm{cm})^{-1}$ (T = 0 K)

[Guo, Murakami, Chen, Nagaosa, PRL100, 096401 (2008)]

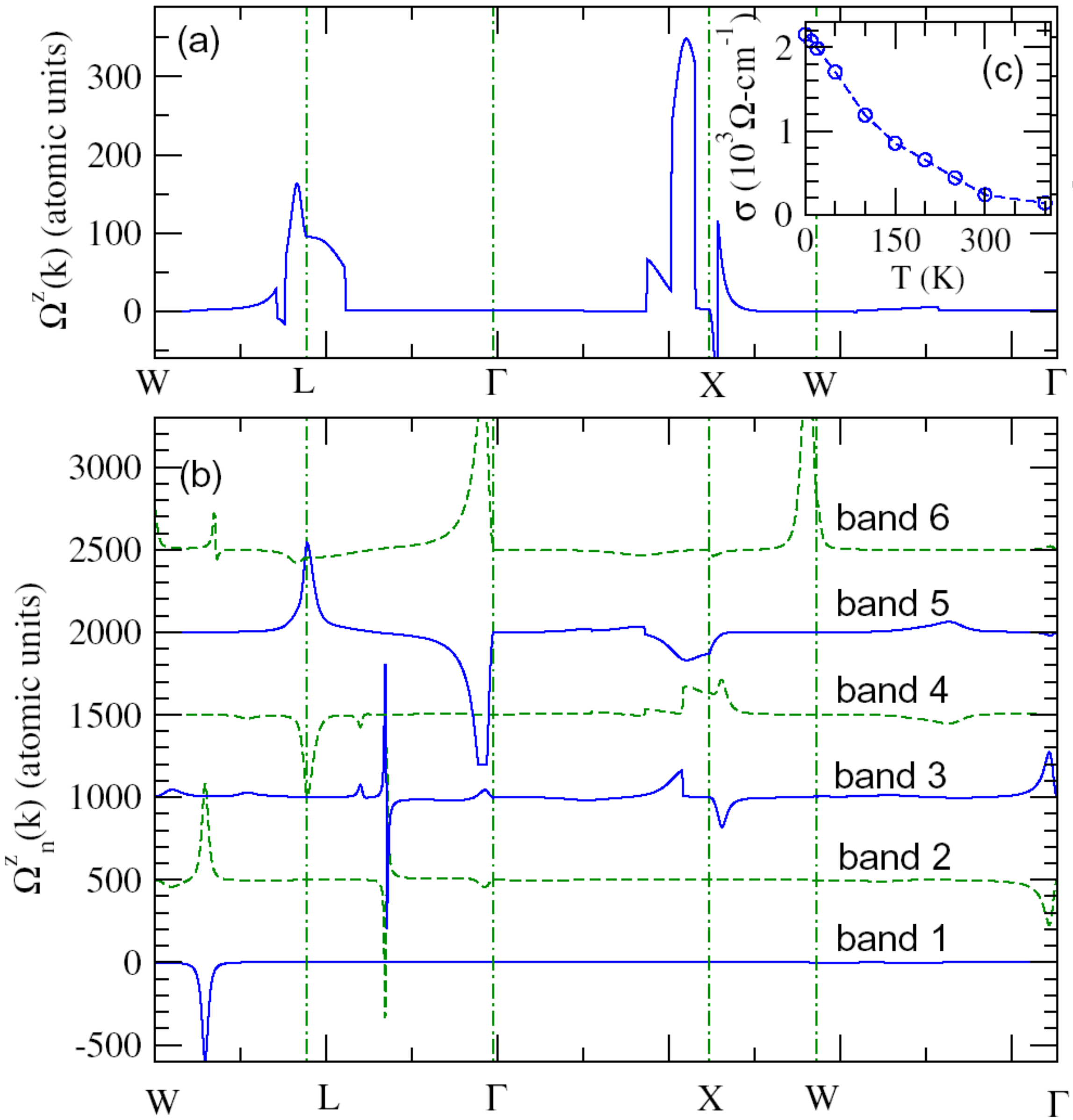

$$\sigma_{xy} = -\frac{e}{\hbar}\sum_{\mathbf{k}}\Omega^z(\mathbf{k}) = \frac{e}{\hbar}\sum_{\mathbf{k}}\sum_n f(\varepsilon_n(\mathbf{k}))\Omega_n^z(\mathbf{k})$$

$$\Omega_n^z(\mathbf{k}) = \sum_{n'\neq n}\frac{2\,\mathrm{Im}\langle \mathbf{k}n|\, j_x^z\,|\mathbf{k}n'\rangle\langle \mathbf{k}n'|\, v_y\,|\mathbf{k}n\rangle}{(\omega_{\mathbf{k}n}-\omega_{\mathbf{k}n'})^2}$$

Pt: σ_{sH} (300K) = 240 $(\Omega\text{cm})^{-1}$

σ_{sH} (exp., RT) = 240 $(\Omega\text{cm})^{-1}$

[Kimura et al PRL98, 156601 (2007)]

Pt: σ_{sH} (0K) = 2200 $(\Omega\text{cm})^{-1}$

σ_{sH} (exp., 5 K) = 1700 $(\Omega\text{cm})^{-1}$

[Morota et al, PRB83, 174405 (2011)]

[Hoffmann, IEEE Trans. Magn. 49 (2013) 5172]

Pt has been widely used as a spin current generator and detector in recent novel spin current experiments, e.g.,

spin Seebeck effect,
[Uchida et al., Nature 455, 778 (2008)]

spin pumping,
[Kajiwara et al., Nature 464, 262 (2010)]

spin Hall switching
[Miron et al., Nature 476, 189 (2011)].

Effect of impurity scattering and two band model analysis

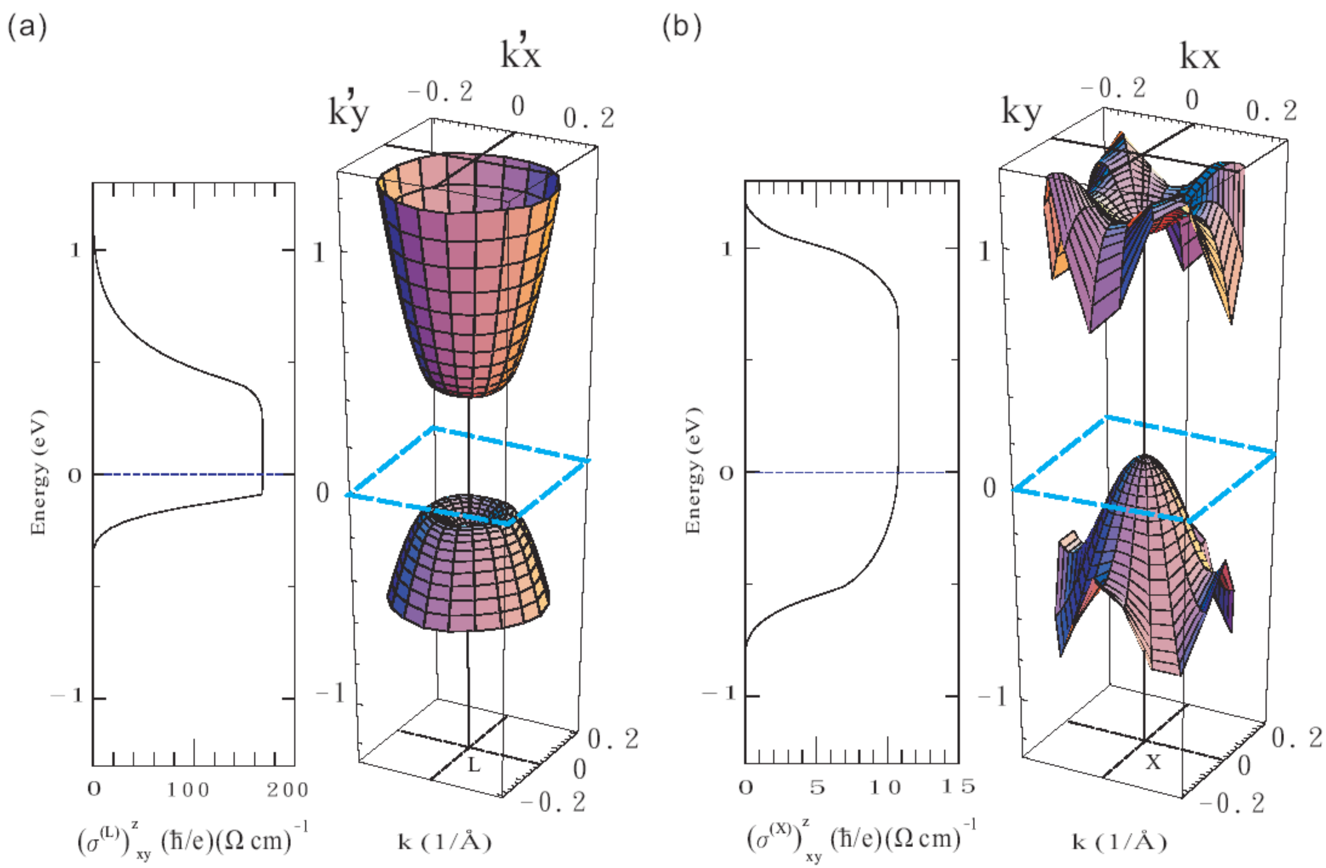

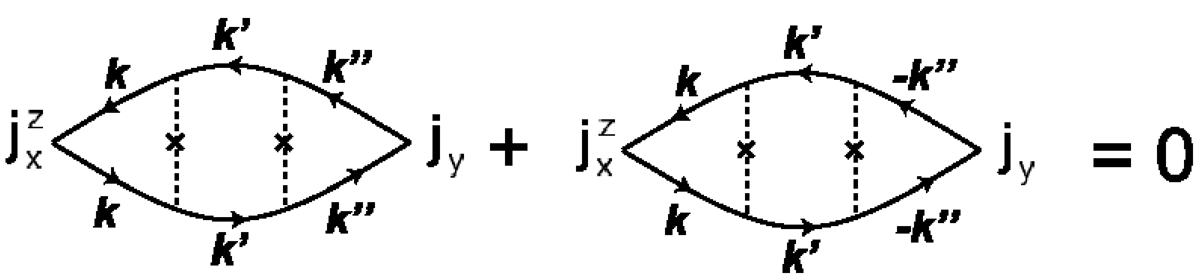

Intrinsic SHE is robust against short-ranged impurity scattering!

3. Intrinsic spin Hall effect in pure Pd, Au and Mo metals

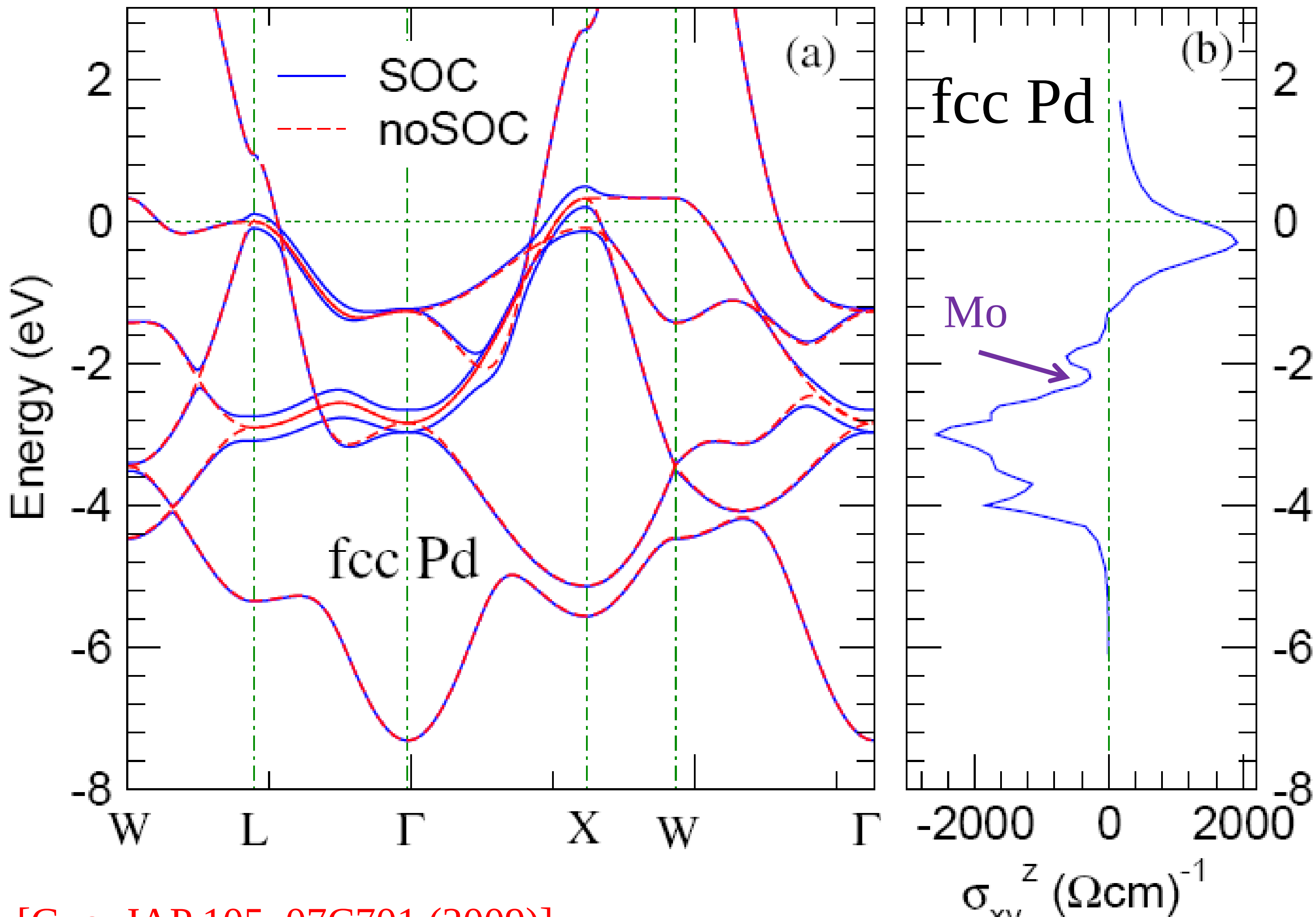

[Guo, JAP 105, 07C701 (2009)]

Pd: σ_{sH} (0 K) = 1400 $(\Omega\text{cm})^{-1}$

σ_{sH} (300K) = 300 $(\Omega\text{cm})^{-1}$

[Morota, et al., JAP 105, 07C712 (2009)]

Mo: σ_{sH} (10 K) = -70 $(\Omega\text{cm})^{-1}$

α_{sH} (10K) = -0.002

Intrinsic spin Hall effect in pure Au and other metals

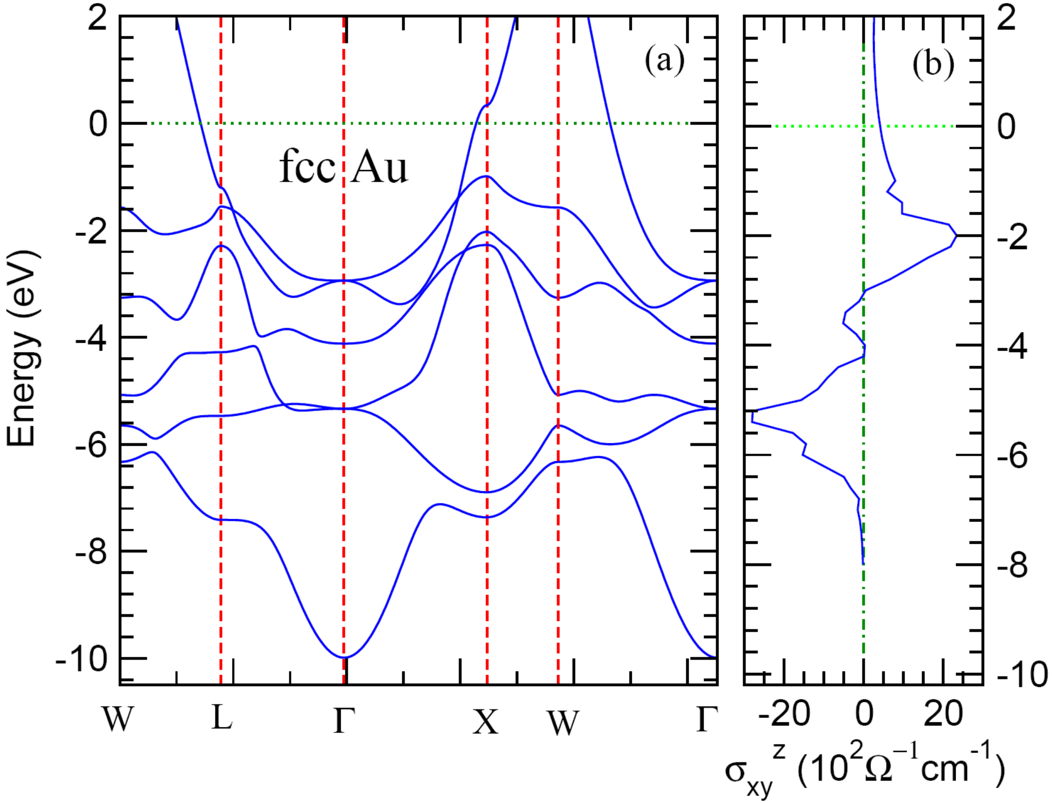

Au: σ_{sH} = 415 (Ωcm)$^{-1}$ (T = 0 K)
= 750 (Ωcm)$^{-1}$ (T = 300 K)

[Guo, JAP 105, 07C701 (2009)]

σ_{sH} (exp., RT) = 882 (Ωcm)$^{-1}$

[b][Mosendz, et al., PRB 82 (2010) 214403]

[a][Morota, et al., PRB 83 (2011) 174405]

	σ_{xy}^{z} (0 K) $[\frac{\hbar}{e}(\mathrm{S/cm})]$	σ_{xy}^{z} (300 K) $[\frac{\hbar}{e}(\mathrm{S/cm})]$
bcc Nb	-164 (-100[a])	-167
bcc Mo	-323 (-230[a])	-407 (-23[b])
bcc Ta	-211 (-11[a])	-156
bcc W	-1009	-1037
fcc Pd	1400[c] (270[a])	350 (256[b])
fcc Pt	2200 (1700[a])	240 (312[b])
fcc Au	415[d]	750 (882[b])

III. Gigantic spin Hall effect in gold and multi-orbital Kondo effect

1. Giant spin Hall effect in perpendicularly spin-polarized FePt/Au devices

[Seki, et al., Nat. Mater. 7 (2008)125]

a

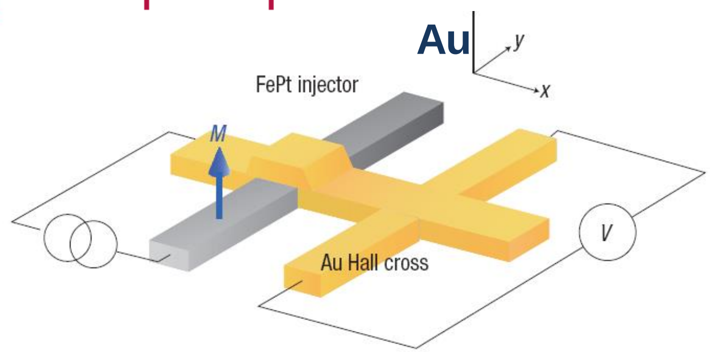

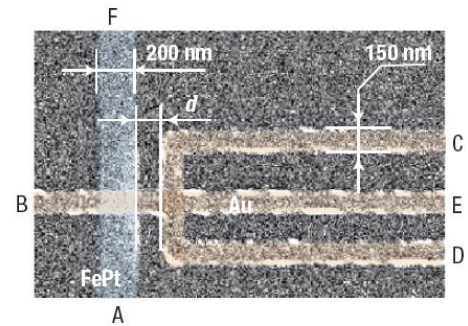

$$\Delta R_{ISHE} = 2\theta_s \frac{\rho_{Au}}{t_{Au}} P \exp(-d/\lambda_{Au})$$

c

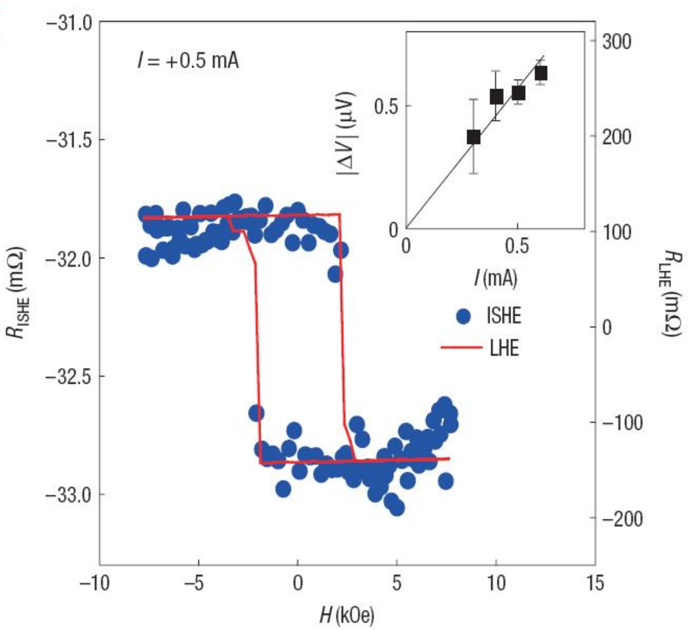

d

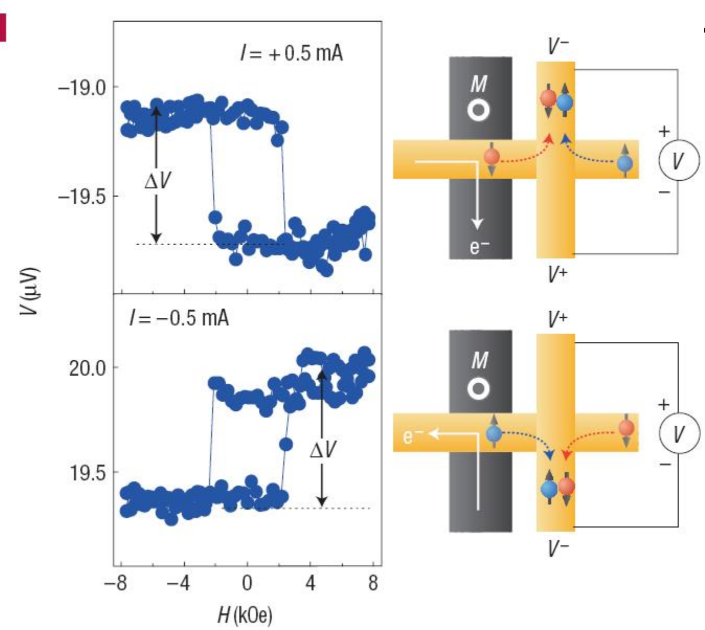

spin Hall angle

$$\alpha_H = \frac{\sigma_{xy}}{\sigma_{xx}} \approx 0.1 \text{ at RT}$$

$$\sigma_{SHE} \approx 10^5\,\Omega^{-1}\mathrm{cm}^{-1}$$

What is the origin of giant spin Hall effect in gold Hall bars?

(i) Surface and interface effect? [Seki, et al., Nat. Mater. 7 (2008)125]

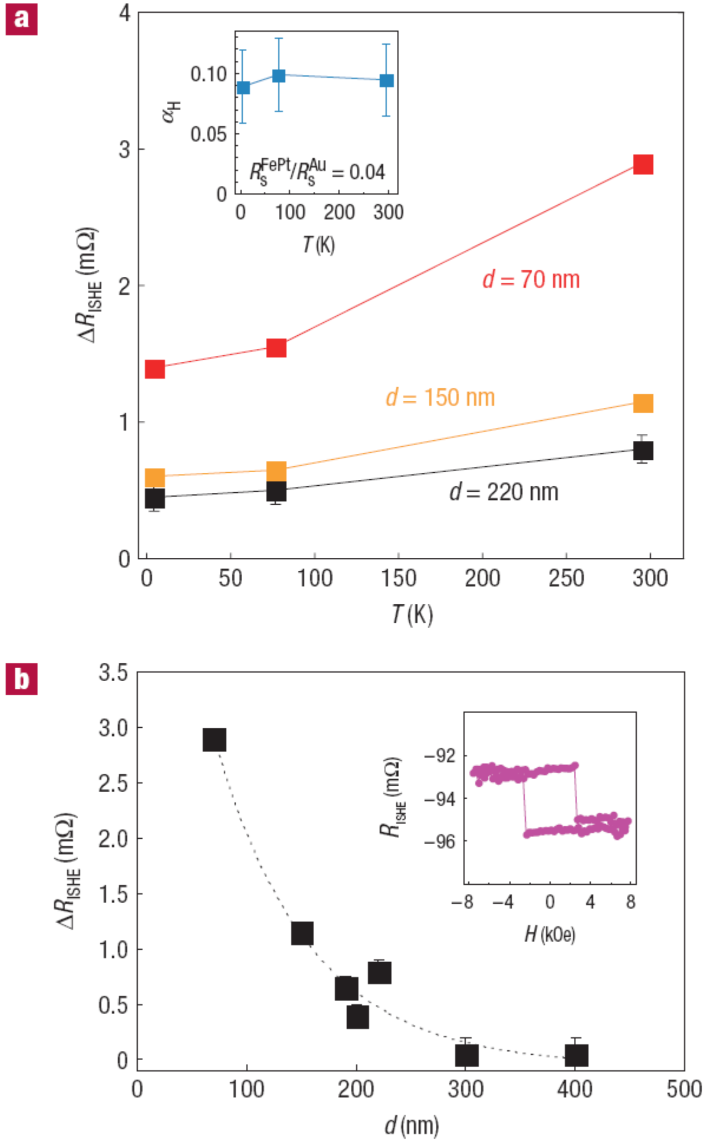

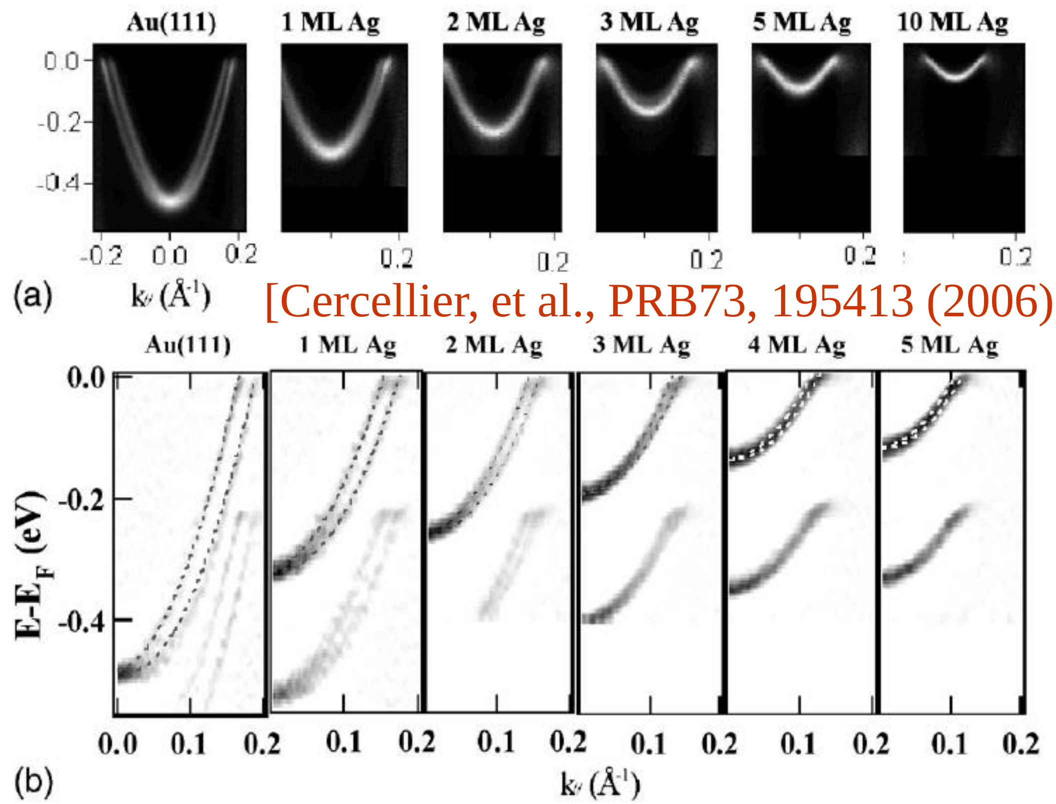

[Cercellier, et al., PRB73, 195413 (2006)]

(ii) Defect and impurity origin ?

Possible impurities: (a) vacancy of Au atom

(b) Pt impurity

(c) Fe impurity

2. Multiorbital Kondo effect in Fe impurity in gold.

[Guo, Maekawa, Nagaosa, PRL 102, 036401 (2009)]

Results of FLAPW calculations
(a) the change in DOS in the 5d bands.
(b) the DOS change is near -1.5 eV.
Nonmagnetic in (a) and (b)
(c) A peak in DOS at the Fermi level and magnetic.

Proposal: Multiorbital Kondo effect in Fe impurity in gold.

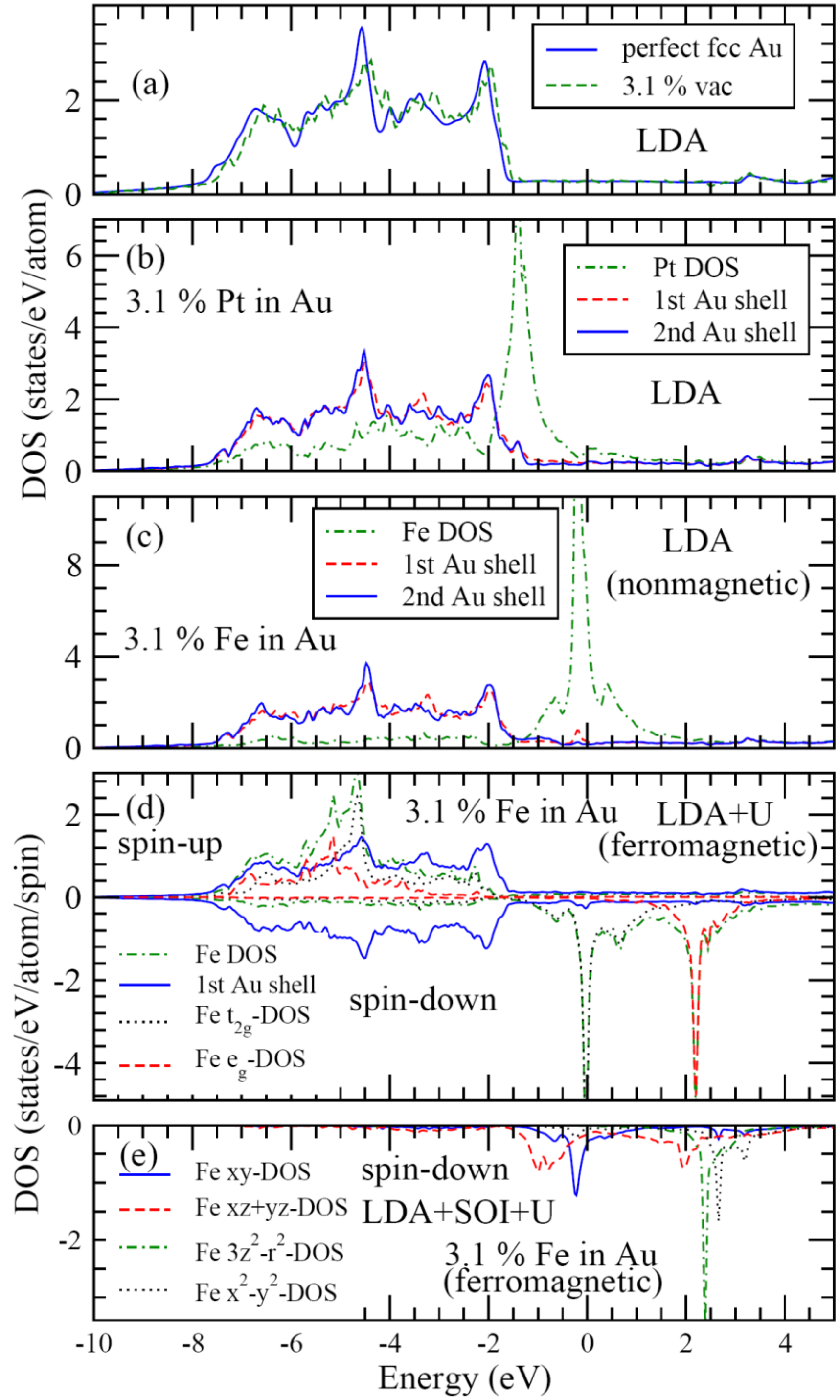

Kondo effect in metals with magnetic impurities

(a classic many-body phenomenon in condensed matter physics)

(1) Resistivity abnormality in Au with dilute magnetic impurities discovered by de Haas et al. in 1930's. [Physica 1 (1934) 1115]

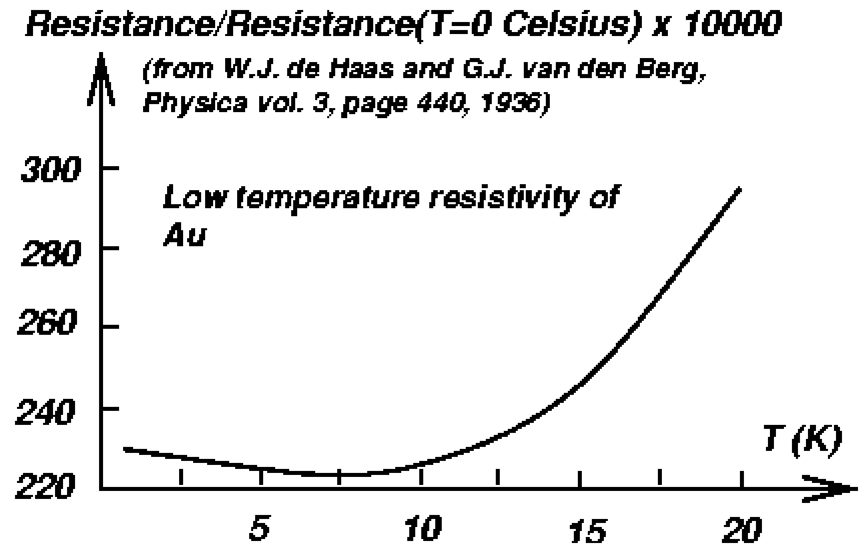

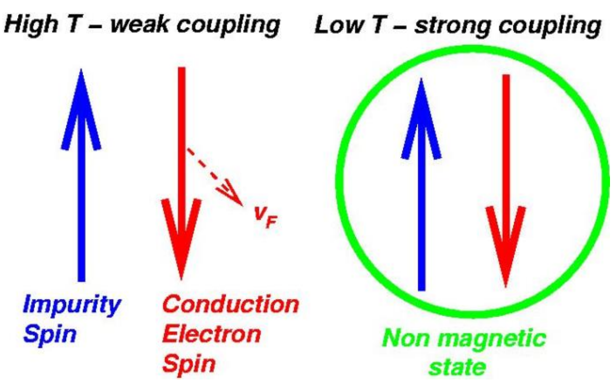

(2) Kondo proposed a (Kondo) model and solved it in the 2nd-order perturbation theory to explain the phenomenon in 1960's. [Prog. Theo. Phys. 32 (1964) 37]

$$H = \sum_{\mathbf{k}\sigma} \varepsilon_k c^{\dagger}_{\mathbf{k}\sigma} c_{\mathbf{k}\sigma} + J\boldsymbol{\sigma}(0)\cdot\mathbf{S}_f \qquad (J>0,\ S_f = 1/2)$$

$$\rho(T) = aT + C_{imp}\rho_0 - C_{imp}\rho_1 \ln T,$$

$$T_{\min} = (\rho_1/5a)^{1/5} C_{imp}^{1/5} \approx T_K \text{ (Kondo temperature)}$$

3. Enhanced SHE by resonant skew scattering in orbital-dependent Kondo effect.

[Guo, Maekawa, Nagaosa, PRL 102, 036401 (2009)]

Extrinsic spin Hall effect due
t

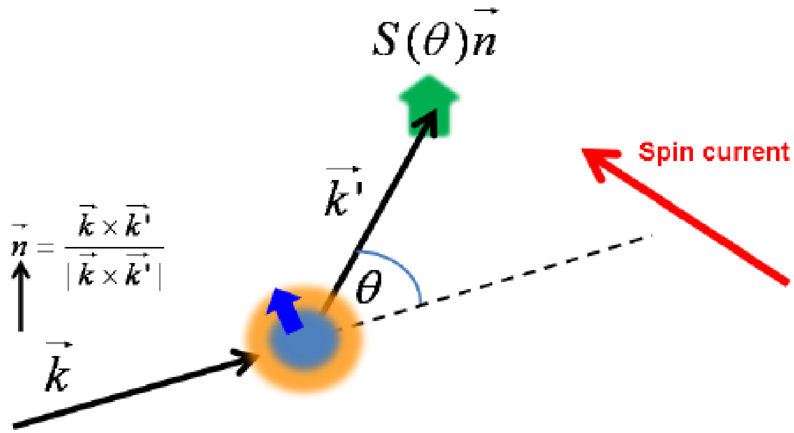

FIG. 1: (color online) The skew scattering due to the spin-orbit interaction of the scatterer and the spin unpolarized electron beam with wavevector $\vec{k}$ with the angle θ with the spin polarization $S(\theta)\vec{n}$ with $\vec{n} = (\vec{k}\times\vec{k}')/|\vec{k}\times\vec{k}'|$.

scattering amplitudes

$$f_\uparrow(\theta) = f_1(\theta)|\uparrow\rangle + ie^{i\varphi} f_2(\theta)|\downarrow\rangle$$
$$f_\downarrow(\theta) = f_1(\theta)|\downarrow\rangle - ie^{-i\varphi} f_2(\theta)|\uparrow\rangle$$

skewness function

$$S(\theta) = \frac{2\mathrm{Im}[f_1^*(\theta) f_2(\theta)]}{|f_1(\theta)|^2 + |f_2(\theta)|^2}$$

spin Hall angle

$$\gamma_S = \frac{\int d\Omega I(\theta) S(\theta)\sin\theta}{\int d\Omega I(\theta)(1-\cos\theta)}$$

$$f_1(\theta) = \sum_l \frac{P_l(\cos\theta)}{2ik}\left[(l+1)\left(e^{2i\delta_l^+}-1\right) + l\left(e^{-2i\delta_l^-}-1\right)\right]$$
$$f_2(\theta) = \sum_l \frac{\sin\theta}{2ik}\left(e^{2i\delta_l^+} - e^{2i\delta_l^-}\right)\frac{d}{d\cos\theta}P_l(\cos\theta).$$

TABLE I: Down-spin occupation numbers of the $3d$-suborbitals of the Fe impurity in Au from LDA+U calculations without SOI and with SOI. The calculated magnetic moments are: $m_s^{Fe} = 3.39\ \mu_B$ and $m_s^{tot} = 3.32\ \mu_B$ without SOI, as well as $m_s^{Fe} = 3.19\ \mu_B$, $m_o^{Fe} = 1.54\ \mu_B$ and $m_s^{tot} = 3.27\ \mu_B$ with SOI. The muffin-tin sphere radius $R_{mt} = 2.65a_0$ (a_0 is Bohr radius) is used for both Fe and Au atoms.

[Guo, Maekawa, Nagaosa, PRL 102, 036401 (2009)]

(a)	xy	xz	yz	$3z^2-r^2$	x^2-y^2
no SOI	0.459	0.459	0.459	0.053	0.053
SOI	0.559	0.453	0.453	0.050	0.128
(b)	$m=-2$	$m=-1$	$m=0$	$m=1$	$m=2$
no SOI	0.256	0.459	0.053	0.459	0.256
SOI	0.138	0.087	0.050	0.819	0.549

Occupation numbers are related to the phase shifts through generalized Friedel sum rule.

$$\theta_s \cong -\frac{3\delta_1(\cos 2\delta_2^+ - \cos 2\delta_2^-)}{9\sin^2\delta_2^+ + 4\sin^2\delta_2^- + 3[1-\cos 2(\delta_2^+ - \delta_2^-)]}$$

$$\theta_s \cong \delta_1 \approx 0.1$$

$$\theta_H \approx 0.001 \sim 0.01$$

[Fert, et al., JMMM 24 (1981) 231]

Physics

Physics **2**, 6 (2009)

Piers Coleman

Department of Physics and Astronomy, Rutgers University

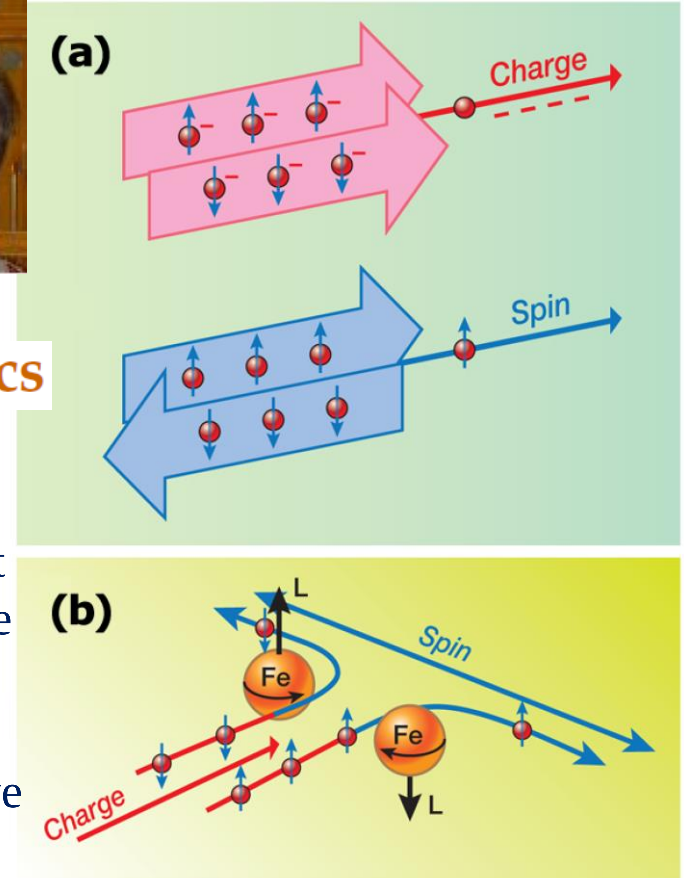

Viewpoint Lending an iron hand to spintronics

In a paper appearing in Physical Review Letters, Guo *et al.*, propose an intriguing theory for this giant spin Hall effect.

Magnetic iron impurities have long been known to have a large effect on the low-T resistivity of gold, via the Kondo effect. If Guo *et al.* are right in their interpretation, the observation of a giant spin Hall effect resulting from the Kondo effect will add a curious new twist to this story. The history of the Kondo effect stretches back over seventy-five years. Despite its long history, the detailed Kondo physics of iron remains a controversial subject.

This is a fascinating state of affairs—a wonderful example of the synergy that is possible between electronics applications and condensed-matter physics. If Guo *et al.* are right, the spin Hall conductivity of gold should scale with the iron concentration, moreover, one might expect iron atoms to produce a large anomalous Hall effect. This could be a very exciting and unexpected turn in the long-standing story of the Kondo effect of iron in gold.

A Viewpoint on:
Enhanced Spin Hall Effect by Resonant Skew Scattering in the Orbital-Dependent Kondo Effect
Guang-Yu Guo, Sadamichi Maekawa and Naoto Nagaosa
Phys. Rev. Lett. **102**, 036401 (2009) – Published January 20, 2009

4. Quantum Monte Carlo simulation of multi-orbital Kondo effect

(1) problems

X-ray magnetic circular dichroism measurements

VOLUME 93, NUMBER 7 PHYSICAL REVIEW LETTERS week ending 13 AUGUST 2004

Direct Observation of Orbital Magnetism in Cubic Solids

W. D. Brewer,[1,*] A. Scherz,[1] C. Sorg,[1] H. Wende,[1] K. Baberschke,[1] P. Bencok,[2] and S. Frota-Pessôa[3]
[1]...t Berlin, Arnimallee 14, D-14195 Berlin-Dahlem, Germany
...ility, BP 220, F-38043 Grenoble Cedex, France
...ulo, CP 66318, 05315-970 São Paulo, São Paulo, Brazil

... 2003; published 11 August 2004)

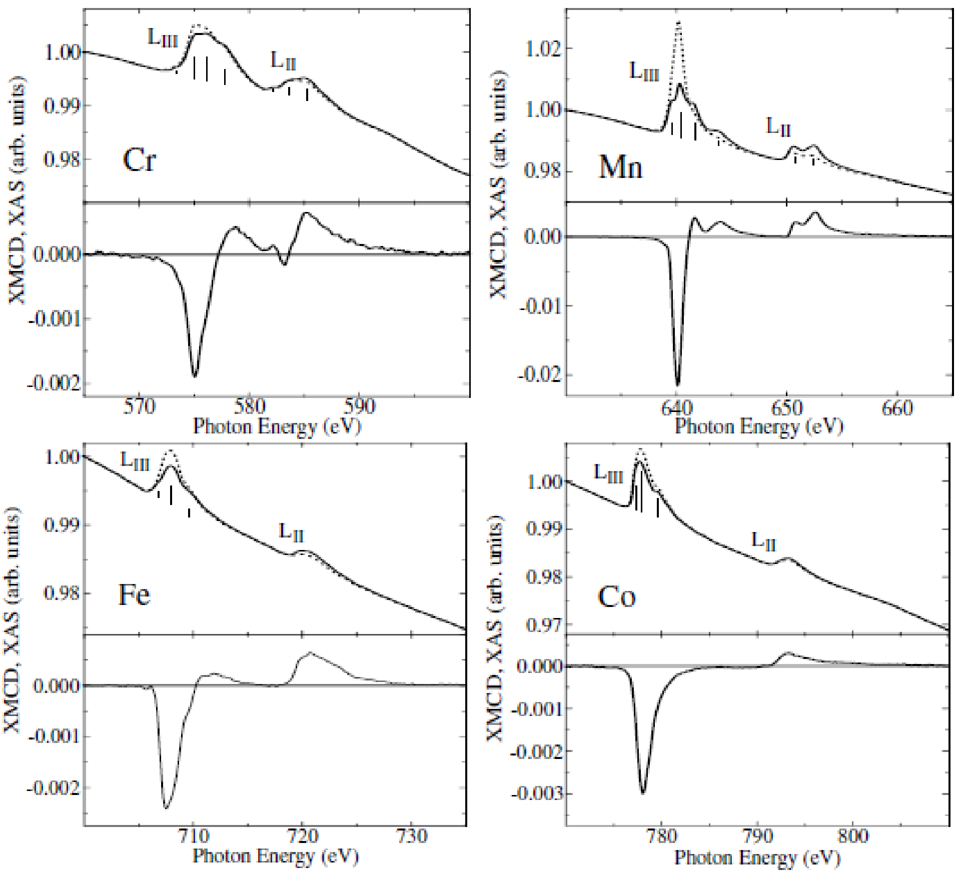

TABLE I. Experimental values of R and the derived orbital/spin magnetic moment ratios for $3d$ impurities in noble metals. The applied field was 7 T, and temperatures T are in K.

Alloy	R	T	$\mu_l/\mu_s^{\mathrm{eff}}$
*Au*Cr (1.0 at. %)	−1.01	18.7	−0.003(30)
*Au*Mn (1.0 at. %)	−0.90	6.8	+0.023(20)
*Cu*Mn (1.0 at. %)	−0.94	6.8	+0.013(20)
*Au*Fe (0.8 at. %)	−0.86	7.2	+0.034(15)
*Au*Co (1.5 at. %)	−0.247	6.8	+0.336(52)

Kondo Decoherence: Finding the Right Spin Model for Iron Impurities in Gold and Silver

T. A. Costi,[1,2] L. Bergqvist,[1] A. Weichselbaum,[3] J. von Delft,[3] T. Micklitz,[4,7] A. Rosch,[4] P. Mavropoulos,[1,2] P. H. Dederichs,[1] F. Mallet,[5] L. Saminadayar,[5,6] and C. Bäuerle[5]

suggests an effective 3-channel Kondo model

$$H = \sum_{k\alpha\sigma} \varepsilon_k c^\dagger_{k\alpha\sigma} c_{k\alpha\sigma} + J \sum_{\alpha} \mathbf{S} \cdot \mathbf{s}_\alpha .$$

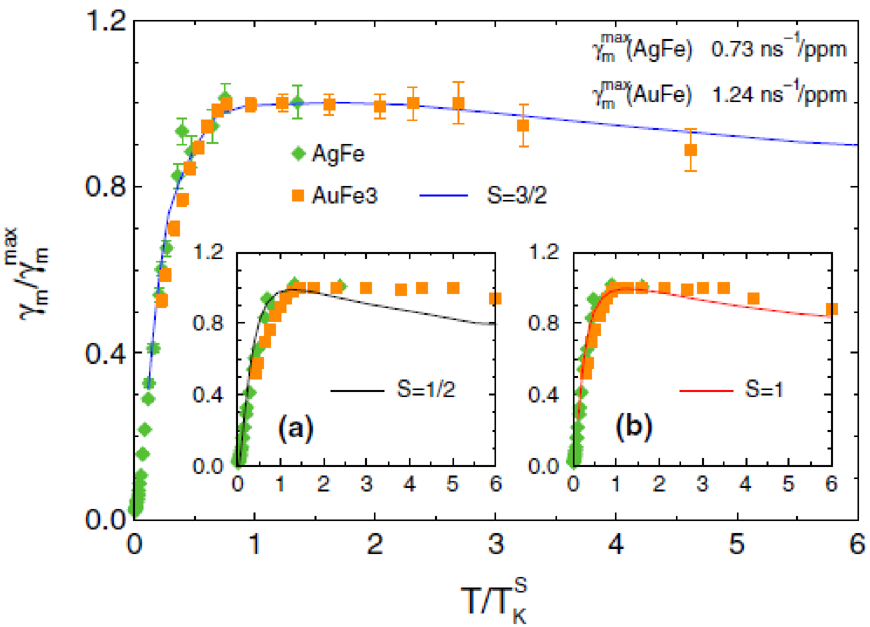

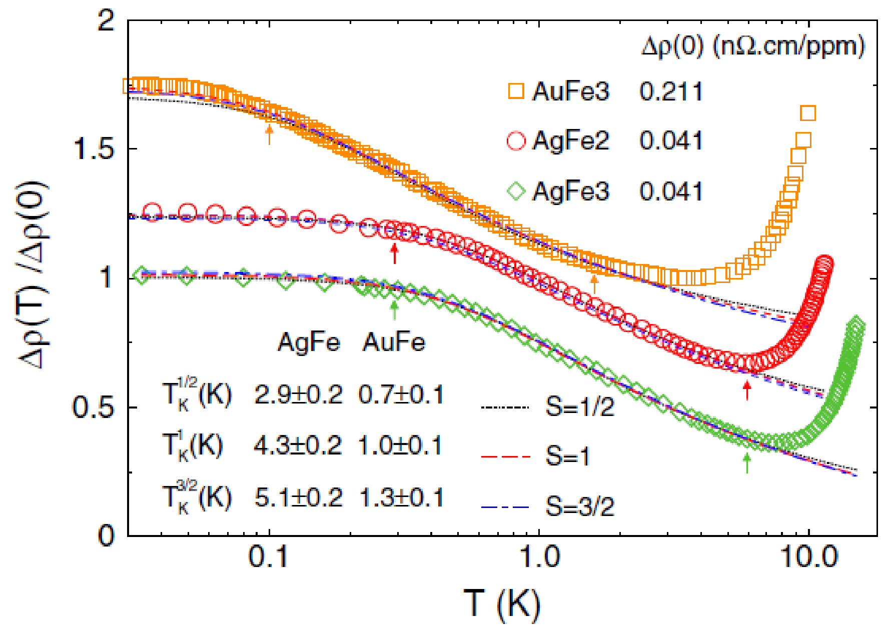

(2) Single-impurity multi-orbital Anderson Model

[Gu, Gan, Bulut, Ziman, Guo, Nagaosa, Maekawa, PRL105 (2010) 086401]

A realistic Anderson model is formulated with the host band structure and the impurity-host hybridization determined by ab initio DFT-LDA calculations.

$$H = \sum_{\alpha,k,\sigma} \varepsilon_{\alpha k} c^{+}_{\alpha k\sigma} c_{\alpha k\sigma} + \sum_{\xi,\sigma} \varepsilon_{\xi} d^{+}_{\xi\sigma} d_{\xi\sigma} + \sum_{\alpha,k,\xi,\sigma} \left(V_{\alpha k\xi} c^{+}_{\alpha k\sigma} d_{\xi\sigma} + h.c. \right)$$

$$+ U \sum_{\xi} n_{\xi\uparrow} n_{\xi\downarrow} + U' \sum_{\sigma,\sigma'} n_{1\sigma} n_{2\sigma'} - J \sum_{\sigma} n_{1\sigma} n_{2\sigma}$$

For host band structure, $\alpha =$ 9 bands (6s, 6p, 5d orbitals of Au) are included.
For impurity-host hybridization, $Au_{26}Fe$ supercell (3X3X3 primitive FCC cell) is considered. $\xi = 5$ (3d orbitals of Fe).

For impurity Fe, one e_g orbital (z^2) and up to two t_{2g} orbitals (xz, yz) are considered with the following parameters.

U = 5 eV, J = 0.9 eV, U'= U – 2J = 3.2 eV

Impurity-host hybridization for FCC $Au_{26}Fe$ (DFT results)

$$V_{\xi\alpha k} = \langle \varphi_\xi | H_0 | \Psi_\alpha(k) \rangle$$
$$= \sum_p a_{\alpha p}(k) \frac{1}{\sqrt{N}} \sum_r e^{ik\cdot r} \langle \varphi_\xi | H_0 | \varphi_p(r) \rangle$$
$$= \frac{1}{\sqrt{N}} \sum_{p,r} e^{ik\cdot r} a_{\alpha p}(k) \langle \varphi_\xi | H_0 | \varphi_p(r) \rangle$$

For FCC $Au_{26}Fe$:
α, p = 9 (6s, 6p, 5d orbitals of Au)
r = 26 (Au_{26})
ξ = 5 (3d orbitals of Fe)

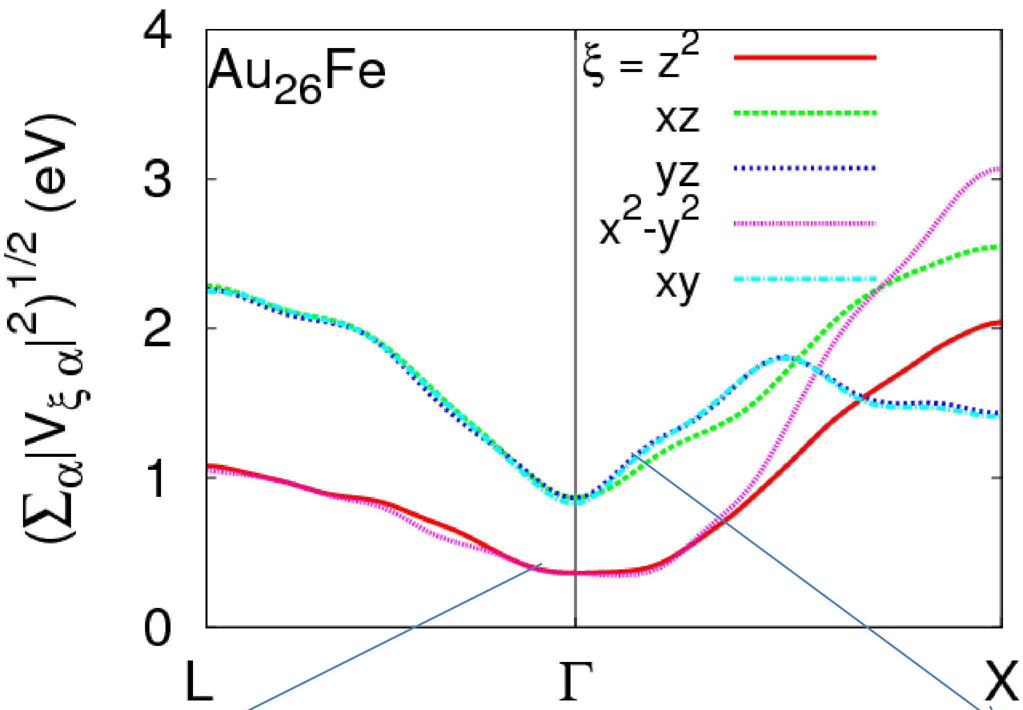

Smaller mixing for e_g

Larger mixing for t_{2g}

- Energy levels for Fe in $Au_{26}Fe$ (DFT results):

t_{2g} : xz, yz, xy : -0.45 eV
e_g : z^2, x^2-y^2 : -0.55 eV

(3) Magnetic behaviors for Fe in Au from QMC simulations

The magnetic behaviors of the Anderson impurity model at finite temperature are calculated by the Hirsh-Fye quantum Monte Carlo (QMC) technique.

[Hirsch and Fye, PRL 56, 2521(1986)]

Universal Kondo susceptibility for the one orbital case

$\varepsilon_d = -U/2$ (Symmetric case, constant DOS).

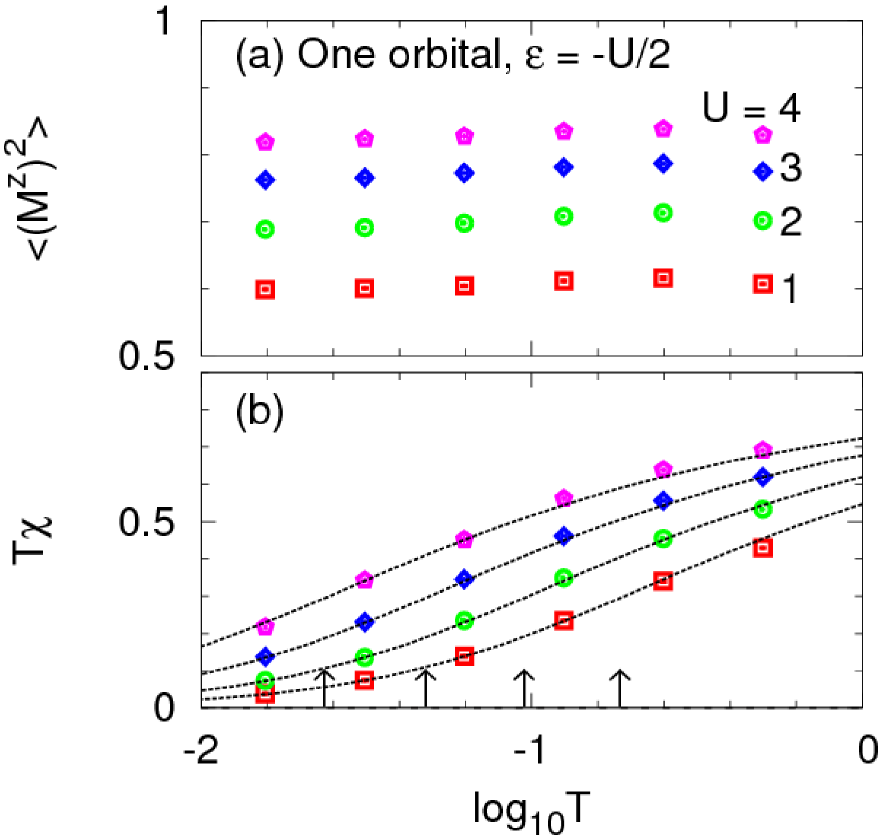

U = 1, 2, 3, 4 eV

T_K = 0.169, 0.0865, 0.0435, 0.0216 eV

1 eV ~ 10,000 K. 0.0216 eV ~ 200 K

$$J_{sd} = \frac{2V^2U}{\varepsilon_d(\varepsilon_d+U)} = -\frac{8V^2}{U}$$

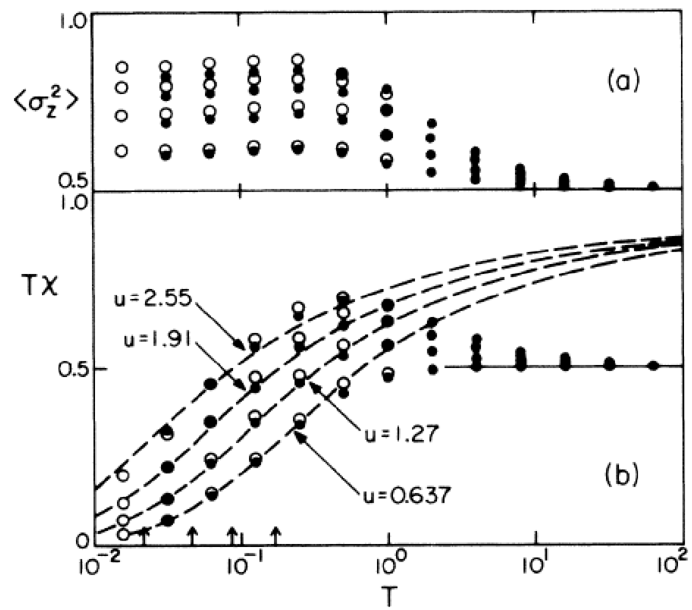

FIG. 2. (a) Local moment $\langle \sigma_z^2 \rangle$ and (b) $T\times$(spin susceptibility) for a single Anderson impurity; $\Delta = 0.5$ and $u = 0.637$, 1.27, 1.91, and 2.55. The closed and open circles correspond to $\Delta\tau = 0.25$ and $\Delta\tau = 0.5$, respectively. The dashed lines are the universal Kondo susceptibility for the four values of T_K given in the text.

$u = U/\pi\Delta$

[Hirsch and Fye, PRL 56, 2521(1986)]

2-orbitals case, e_g and t_{2g}

$$\xi = 1 : z^2,$$

$$\xi = 2 : xz.$$

Local moment

$$M_\xi^z = n_{\xi\uparrow} - n_{\xi\downarrow},$$

In

$$\chi_\xi = \int_0^\beta d\tau \langle M_\xi^z(\tau) M_\xi^z(0)\rangle,$$

Occupation number

$$n_\xi = n_{\xi\uparrow} + n_{\xi\downarrow},$$

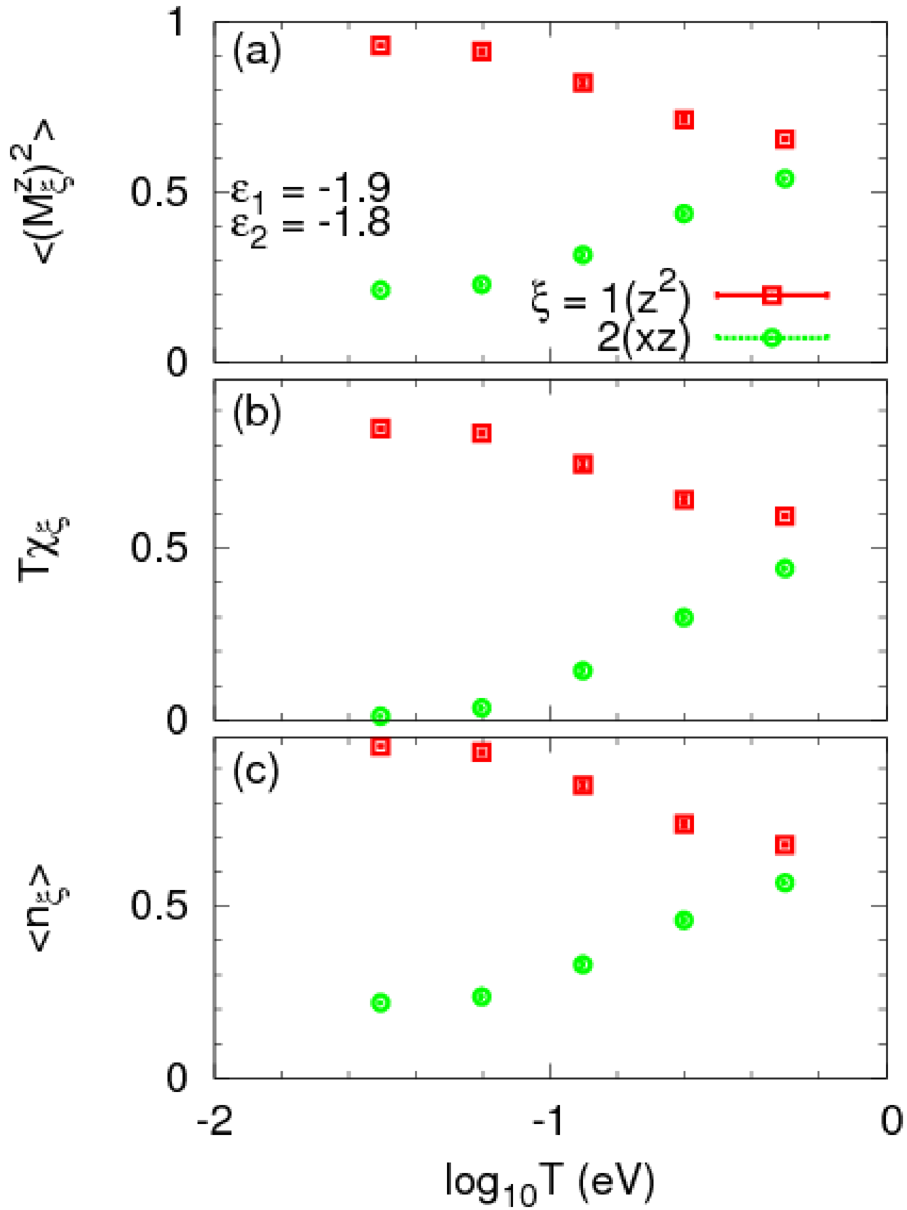

3-orbitals case, e_g and t_{2g}

3-Orbitals case

$$\xi = 1 : z^2,$$
$$\xi = 2 : -\frac{1}{\sqrt{2}}(xz - iyz) : p_1 : l = 1, m = 1;$$
$$\xi = 3 : -\frac{1}{\sqrt{2}}(xz + iyz) : p_{-1} : l = 1, m = -1.$$

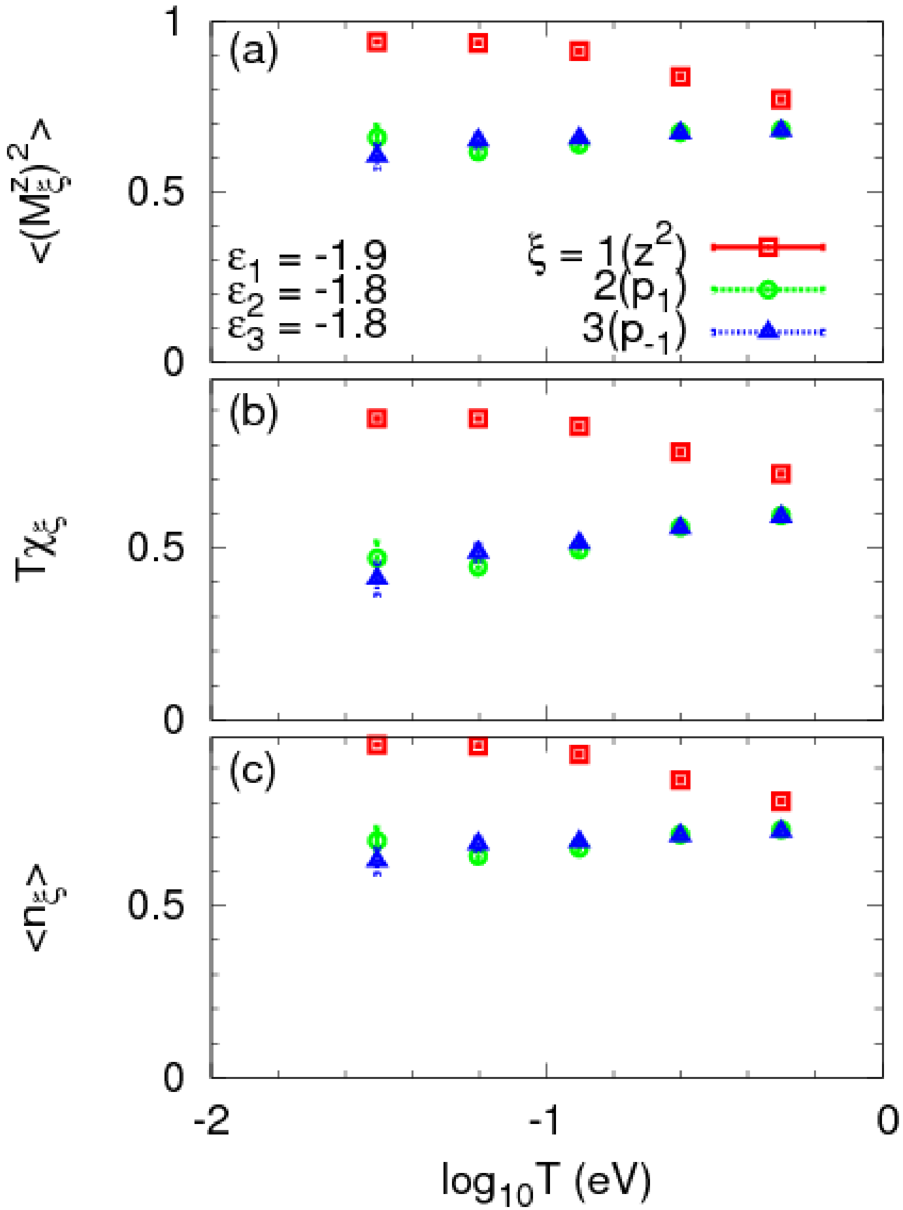

(4) Spin-orbit interaction within t_{2g} oribtals for Fe in Au

[Gu, Gan, Bulut, Ziman, Guo, Nagaosa, Maekawa, PRL105 (2010) 086401]

Ising-type spin-orbit interaction for *p*-electrons: l =1, m =1,0,-1.

$$H_{so} = (\lambda/2) \sum_{m,m',\sigma,\sigma'} d^{\dagger}_{m\sigma} (\mathbf{l})_{mm'} \cdot (\sigma)_{\sigma\sigma'} d_{m'\sigma'} ,$$

$$H_{so} = (\lambda/2) \sum_{m,\sigma} d^{\dagger}_{m\sigma} (\mathbf{l})^{z}_{mm} (\sigma)^{z}_{\sigma\sigma} d_{m\sigma} .$$

$$l^z = \begin{pmatrix} 1 & 0 & 0 \\ 0 & 0 & 0 \\ 0 & 0 & -1 \end{pmatrix}, \sigma^z = \begin{pmatrix} 1 & 0 \\ 0 & -1 \end{pmatrix},$$

$$H_{so} = (\lambda/2) \left(n_{1\uparrow} - n_{1\downarrow} - n_{-1\uparrow} + n_{-1\downarrow} \right) ,$$

T = 350 K, = 75 meV

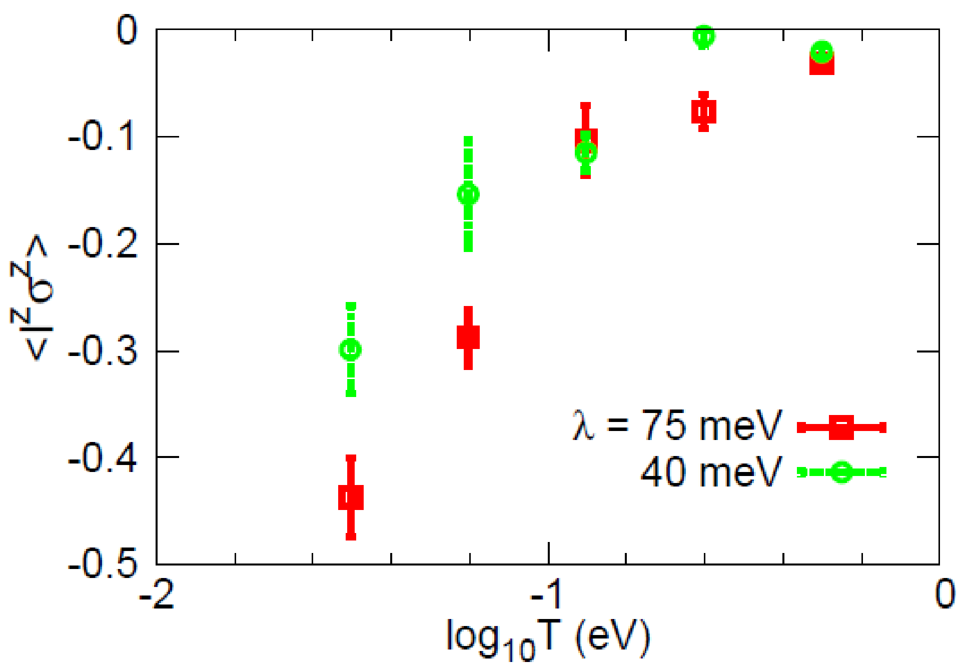

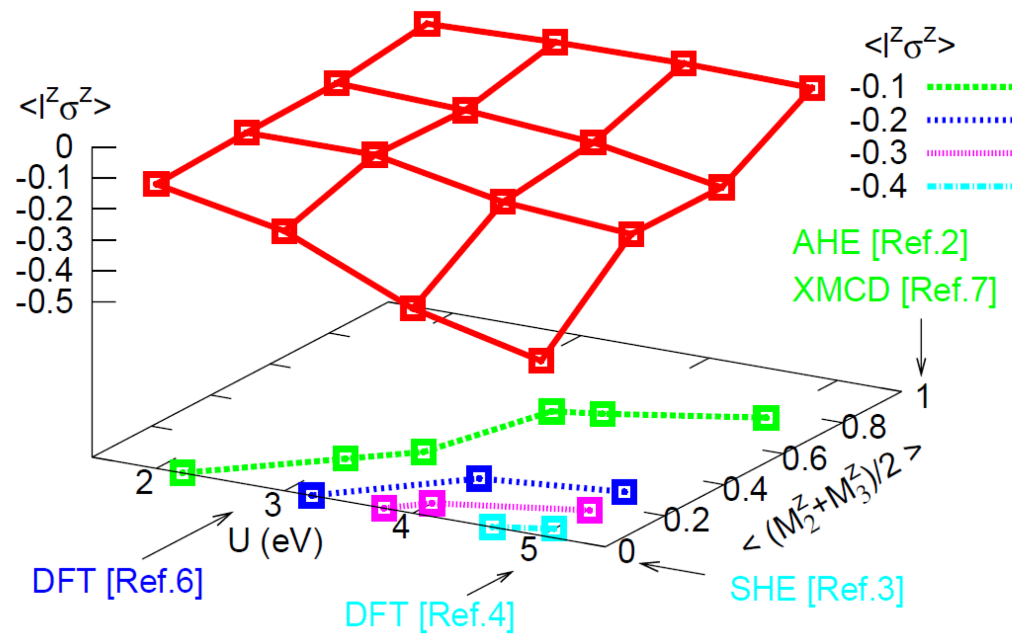

(5) Estimation of spin Hall angle for Fe impurity in Au

$$\theta_s \cong -\frac{3\delta_1(\cos 2\delta_2^+ - \cos 2\delta_2^-)}{9\sin^2\delta_2^+ + 4\sin^2\delta_2^- + 3[1-\cos 2(\delta_2^+ - \delta_2^-)]}$$

Since we consider only two t_{2g} orbitals with $\ell_z = \pm 1$, the SOI within the t_{2g} orbitals gives rise to the difference in the occupation numbers between the parallel (n_P) and anti-parallel (n_{AP}) states of the spin and angular momenta. These occupation numbers are related to the phase shifts δ_P and δ_{AP}, through generalized Friedel sum rule, respectively, as $n_{P(AP)} = \delta_{P(AP)}/\pi$, and $\pi < \ell_z\sigma_z > = \delta_P - \delta_{AP}$, $\pi < n_2 > = \pi < n_3 >= \delta_P + \delta_{AP}$.

Putting $< \ell_z\sigma_z >= -0.44$ for $\lambda = 75$ meV, and $< n_2 > = <n_3>= 0.65$, we obtain $\delta_P = 1.35$ and $\delta_{AP} = 2.73$.

Taking into account the estimate $\sin \delta_1 \sim= 0.1$, $\theta_s \sim= 0.06$ is thus obtained.

[Seki, et al., Nat. Mater. 7 (2008)125]

$\theta_s \sim= 0.11$ (exp.)

Influence of Fe Impurity on Spin Hall Effect in Au

Isamu Sugai[1], Seiji Mitani[2], and Koki Takanashi[1]

[1]Institute for Materials Research, Tohoku University, Sendai 980-8577, Japan
[2]National Institute for Materials Science, Tsukuba 305-0047, Japan

We investigated the influence of Fe impurity on spin Hall effect in Au using multi-terminal devices consisting of an FePt perpendicular spin polarizer and a Au Hall cross with different Fe impurity concentrations. As the Fe impurity concentration was increased in the range of 0–0.95 at.%, the resistivity of Au doped with Fe increased and the spin diffusion length decreased from 35 nm to 27 nm. On the other hand, the spin Hall angle for Au doped with Fe, evaluated from the spin injector-Hall cross distance dependence of spin Hall signals, was approximately 0.07, independent of the Fe concentration. The experimental results provide important information for understanding the mechanism of the large spin Hall effect.

PARAMETERS OF $P_{\underline{\mathrm{Au}}\mathrm{Fe}}$, $R_s^{\underline{\mathrm{Au}}\mathrm{Fe}}$, $\lambda_{\underline{\mathrm{Au}}\mathrm{Fe}}$, P AND α_H OBTAINED FOR THE PRESENT FePt/Au DEVICES

Skew scattering
$\theta_s \sim 0.07$,
independent of
Fe concentration.

	$\rho_{\underline{\mathrm{Au}}\mathrm{Fe}}$ [μΩ·cm]	$\lambda_{\underline{\mathrm{Au}}\mathrm{Fe}}$ [nm]	$R_s^{\underline{\mathrm{Au}}\mathrm{Fe}}$ [Ω]	P	α_H
Non-doped Au	3.6	35 ± 4	1.1	0.038	0.07 ± 0.02
$Au_{99.58}Fe_{0.42}$	4.3	33 ± 3	1.3	0.034	0.07 ± 0.01
$Au_{99.05}Fe_{0.95}$	7.0	27 ± 3	1.7	0.027	0.07 ± 0.03

IV. Conclusions and On-going Work

Conclusions

1. *Ab initio* calculations reveal that intrinsic SHC in Pt is large ~2000 $(\Omega\text{cm})^{-1}$, due to the resonant contribution from the spin-orbit splitting of the *d* bands at high-symmetry *L* and *X* points near the Fermi level. The calculated intrinsic SHC in Mo, Pd, Pt and Au agree well with recent experimental results.

2. LDA+U electronic structure indicates that Fe in Au may undergo an orbital-dependent Kondo effect, where the t_{2g} orbitals are in the mixed-valence region while e_g orbitals are in the Kondo limit. This proposal is corroborated by recent QMC calculations.

3. The enhanced spin-orbit interaction by the electron correlation in the t_{2g} orbitals leads to the large spin Hall effect which explains the gigantic spin Hall angle θ_S = ~0.1 observed recently in Au with Fe impurities.

On-going Work

1. Drawbacks of QMC:
a. Applicable only in high temperatures;
b. No information about dynamical properties (Green function and spectral functions, and thus transport coefficients cannot be evaluated.

2. Multi-orbital Kondo effect with SOC by NRG calculations:
a. A grand plan cannot be implemented at moment.
b. Thus, we are performing NRG calculations for 1- and 2-channel pseudo-gap Anderson model to study Kondo effect in graphene and graphene-like system to gain experience and expertise.

1-channel Kondo effect in graphene from NRG calculations

[Lo, Guo, Anders, PRB 89 (2015) 195424]

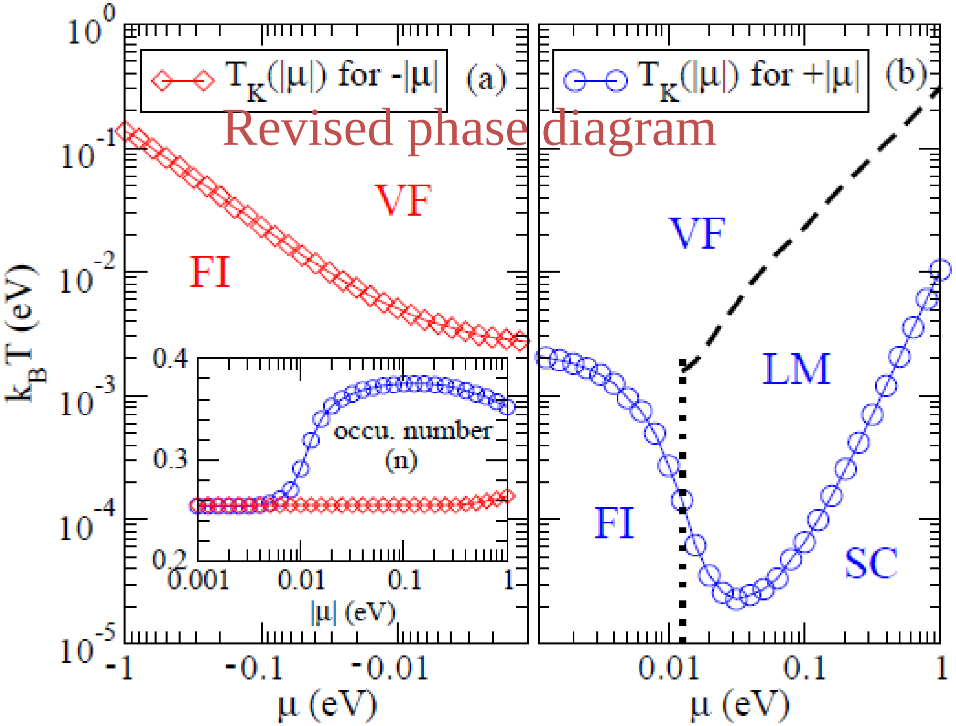

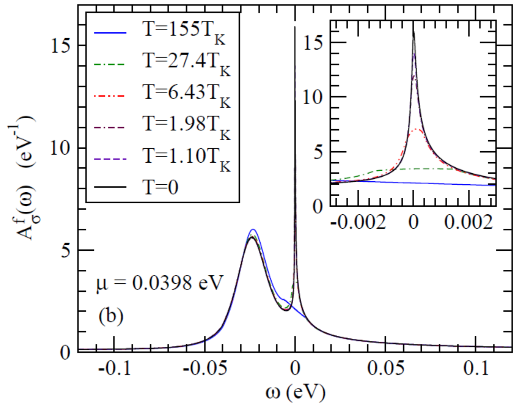

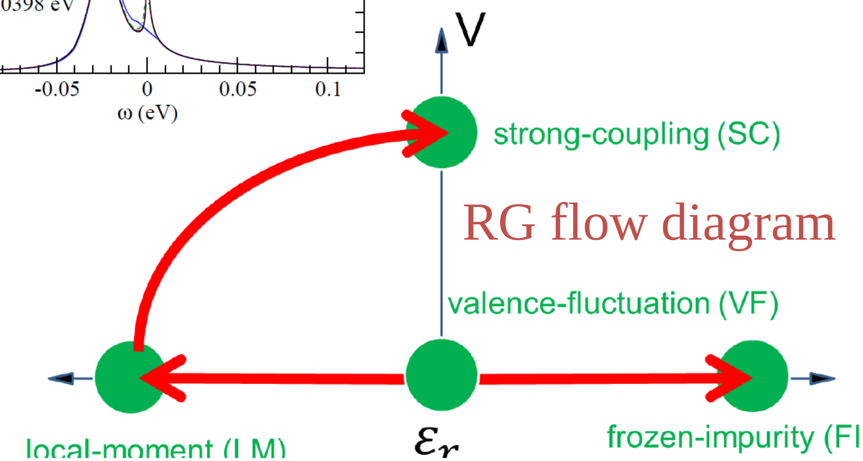

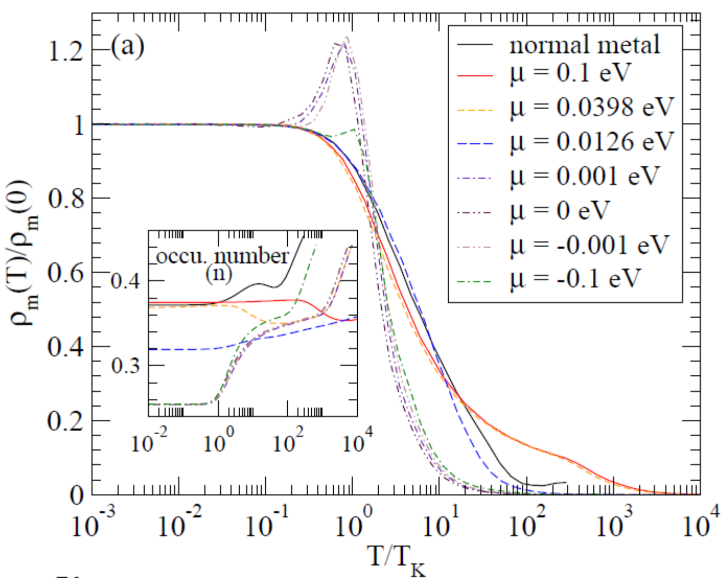

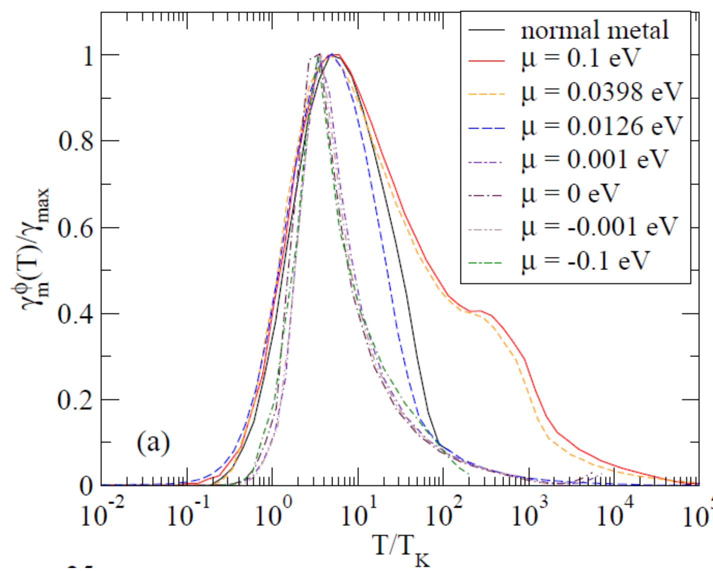

2 channel Kondo effect in pseudogap Anderson model from NRG calculations

$\rho_c(\omega) \propto |\omega - \mu_F|^r \quad (0<r<1)$ [Wu, Wang, Guo, Anders, Chung, JPCM (submitted 2016/01)]

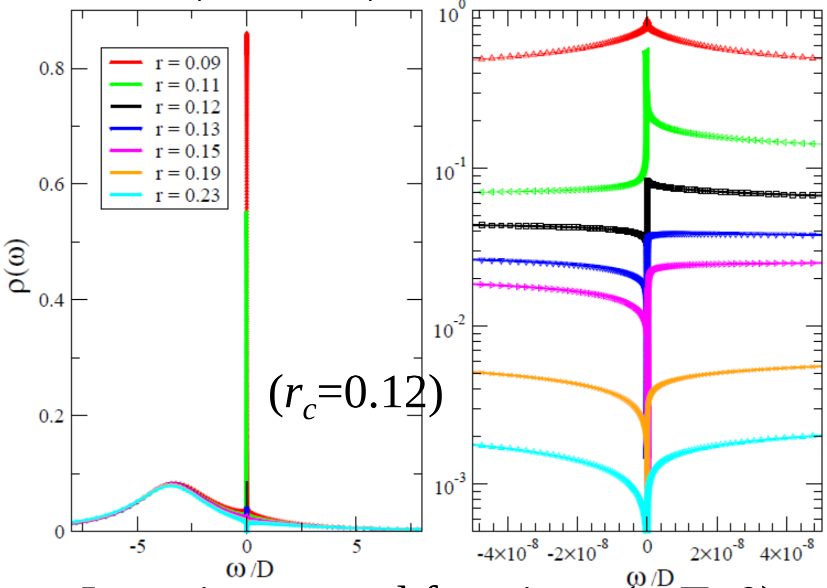

Impurity spectral function ρ(ω,T=0)

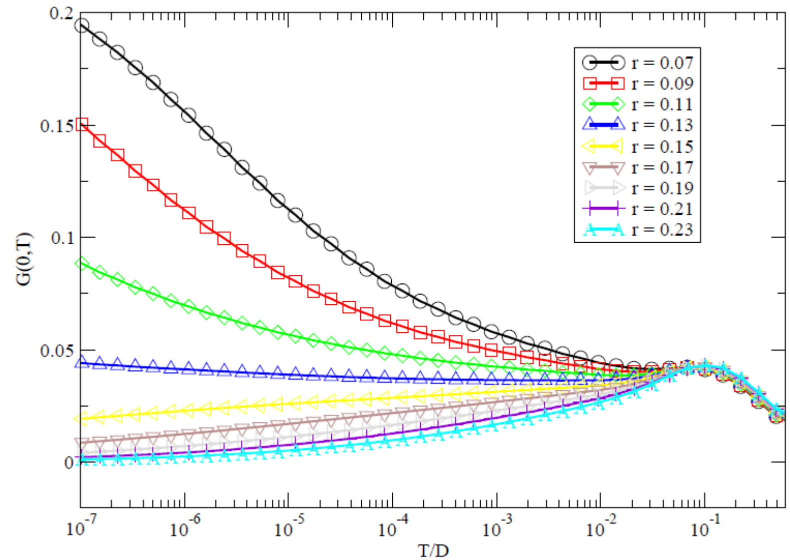

Conductance G(0,T) vs. temperature (T)

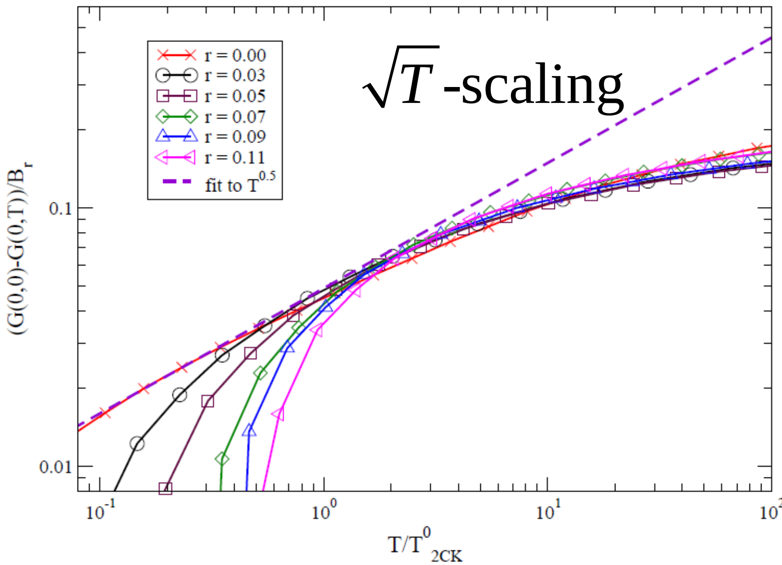

Conductance (G(0,0)-G(0,T))/B vs T/T^0_{2cK}.

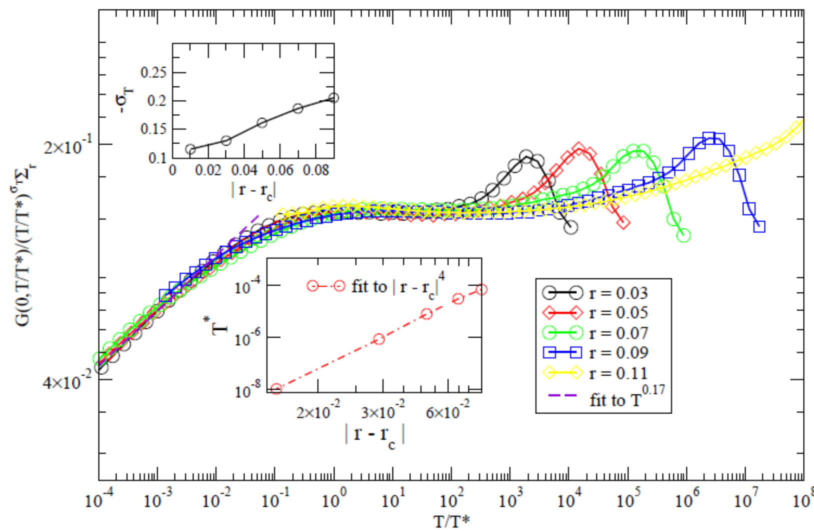

Universal scaling in G(0,T/T*) vs T/T*.

Acknowledgements:

Collaboration:

Qian Niu (UT Austin)
Naoto Nagaosa (Tokyo U.)
Bo Gu, Sadamichi Maekawa (JAEA, Tokai)
Tsung-Wei Chen (Nat'l Taiwan U.)
Shuichi Murakami (Tokyo Inst. Techno.)
Frithjof Anders (UT Dortmund)
Po-Wei Lo, Xiao-Qun Wang (Nat'l Taiwan U.)

Financial Support:

Ministry of Science and Technology
National Center for Theoretical Sciences